# The mycobacterial *guaB1* gene encodes a guanosine 5′-monophosphate reductase with a cystathionine-β-synthase domain

Zdeněk Knejzlík, Michal Doležal (ID), Klára Herkommerová, Kamila Clarova, Martin Klíma (ID), Matteo Dedola (ID), Eva Zborníková, Dominik Rejman and Iva Pichová (ID)

Institute of Organic Chemistry and Biochemistry of the Czech Academy of Sciences, Prague, Czech Republic

Mycobacteria express enzymes from both the *de novo* and purine-salvage pathways. However, the regulation of these processes and the roles of individual metabolic enzymes have not been sufficiently detailed. Both *Mycobacterium tuberculosis* (Mtb) and *Mycobacterium smegmatis* (Msm) possess three *guaB* genes, but information is only available on *guaB2*, which encodes an essential inosine 5′-monophosphate dehydrogenase (IMPDH) involved in *de novo* purine biosynthesis. This study shows that *guaB1*, annotated in databases as a putative IMPDH, encodes a guanosine 5′-monophosphate reductase (GMPR), which recycles guanosine monophosphate to inosine monophosphate within the purine-salvage pathway and contains a cystathionine-β-synthase domain (CBS), which is essential for enzyme activity. GMPR activity is allosterically regulated by the ATP/GTP ratio in a pH-dependent manner. Bioinformatic analysis has indicated the presence of GMPRs containing CBS domains across the entire Actinobacteria phylum.

## Introduction

Purines, as the basic building block of nucleic acids, energy metabolites, cofactors, signalling molecules and metabolic intermediates, are essential components of living organisms. In most organisms, there are two pathways for purine nucleotide biosynthesis: (a) the *de novo* pathway, in which nucleotides are synthesised from 5′-phospho-α-D-ribose-1′-diphosphate (PRPP) in a series of reactions; and (b) the salvage pathway, in which corresponding purine nucleotides, nucleosides and free bases are interconverted (Fig. 1A) [1]. Mycobacteria, including *Mycobacterium smegmatis* (Msm) and *Mycobacterium tuberculosis* (Mtb), express enzymes from both the *de novo* and purine-salvage pathways.

However, the interdependence and regulation of these processes during different stages of the mycobacterial life cycle remain unclear [2]. Several *de novo* pathway enzymes have recently been shown to be expressed in dependence on the cell cycle progression in Mtb [3]. On the other hand, the enzyme amidophosphoribosyltransferase (PurF, EC 2.4.2.14), catalysing the first step of purine *de novo* synthesis, is required for the late stationary phase adaptation during hypoxia in Msm [4]. Nevertheless, detailed data on purine metabolism in mycobacteria are still scarce. It is generally supposed that the less energetically demanding salvage pathway contributes to the purine homeostasis under low energy

**Abbreviations**

CBS, cystathionine-β-synthase domain; GMPR, guanosine 5′-monophosphate reductase; IMPDH, inosine 5′-monophosphate dehydrogenase; Msm, *Mycobacterium smegmatis*; Mtb, *Mycobacterium tuberculosis*.
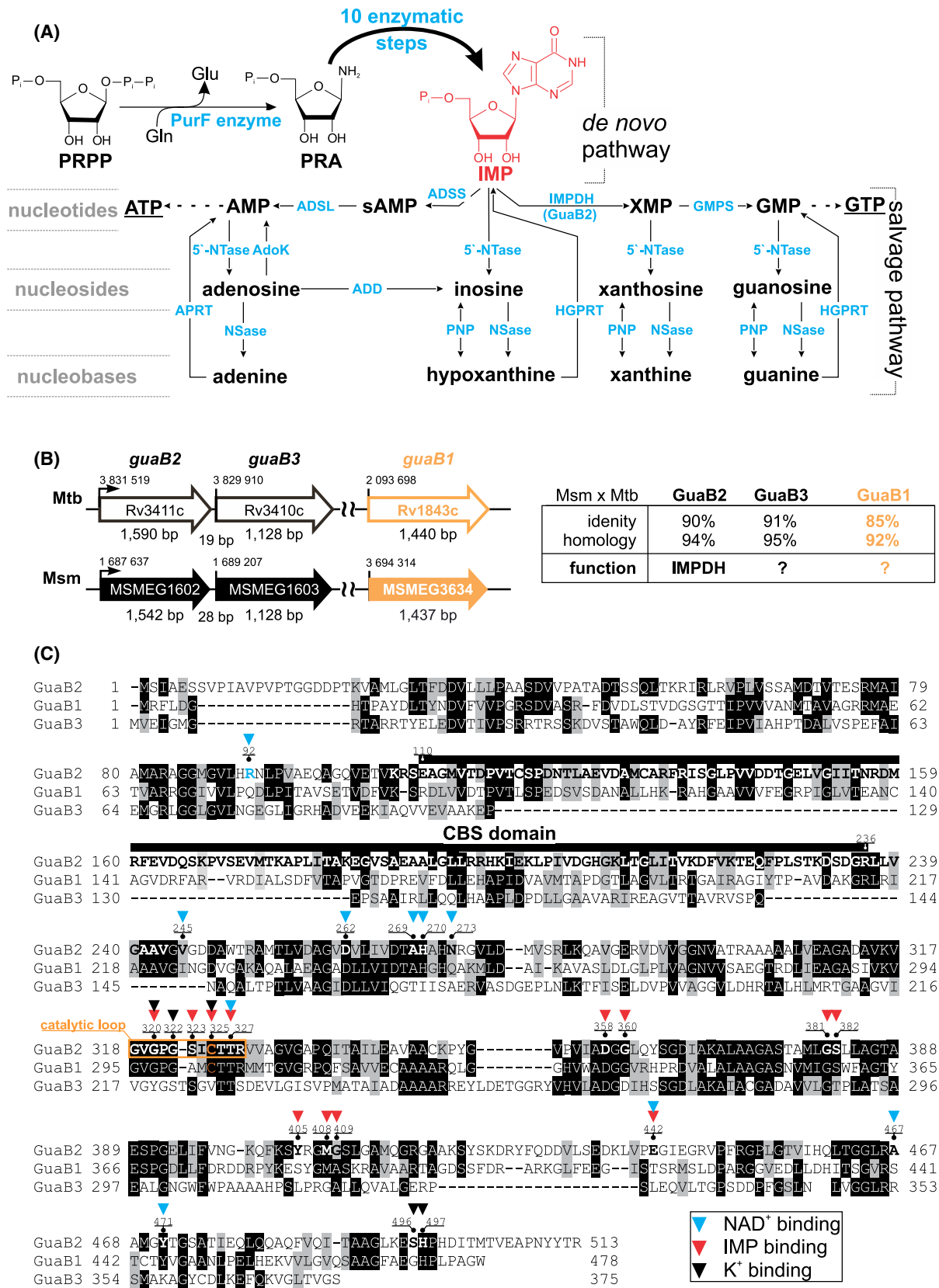
**Fig. 1.** (A) A simplified scheme of purine metabolism in mycobacteria. In the first step of the *de novo* purine biosynthesis, the enzyme amidophosphoribosyltransferase (PurF) catalyses the conversion of 5-phospho-α-D-ribose 1-diphosphate (PRPP) to 5-phospho-β-D-ribosylamine (PRA). Subsequently, 10 enzymatic reactions are required for the generation of inosine 5′-phosphate (IMP, in red). IMP is then converted to adenine and guanine nucleotides in two independent parallel step reactions. Individual purine nucleotides, nucleosides and nucleobases could be interconverted via the salvage pathway. Enzymes are labelled in light blue. ADSS, adenylosuccinate synthase (PurA); ADSL, adenylosuccinate lyase (PurB); IMPDH, IMP dehydrogenase (GuaB2); GMPS, GMP synthase (GuaA); 5′-NTase, 5′-nucleotidase; AdoK, adenosine kinase; NSase, purine nucleoside hydrolase (IunH); PNP, purine nucleoside phosphorylase (DeoD); ADD, adenosine deaminase; APRT, adenine phosphoribosyltransferase; HGPRT, guanine phosphoribosyltransferase. (B) A comparison of the genomic localisation of *guaB1*, *guaB2* and *guaB3* genes. The chromosome position of *guaB1*, *guaB2* and *guaB3* genes in Mtb and Msm (left). The homology and identity of the individual genes are shown in the table on the right. (C) The Msm GuaB1 (GenBank # ABK74721), GuaB2 (GenBank # ABK69632) and GuaB3 (GenBank # ABK75325) amino acid alignment by CLUSTAL Ω software. Identical amino acid residues are marked by black and similar by grey boxes. The amino acid residues involved in $K^+$, IMP and $NAD^+$ binding in the structure of the GuaB2ΔCBS complex with XMP and $NAD^+$ [13] are shown by black, red and blue arrows respectively. The GuaB2 catalytic loop is framed in orange, the catalytic Cys325 residue is in orange and the amino acid sequence of the CBS domain (Glu110–Arg236) is underlined by a black line.

availability and is involved in extracellular purine utilisation in mycobacteria [5,6].

The hub metabolite for the biosynthesis of guanosine monophosphate (GMP) and adenosine monophosphate (AMP) is inosine monophosphate (IMP). In mycobacteria, IMP is converted into xanthosine monophosphate (XMP) by an $NAD^+$-dependent inosine monophosphate dehydrogenase (IMPDH, EC 1.1.1.205) encoded by the *guaB2* gene (*MSMEG_1602* in Msm and *Rv3411c* in Mtb). This reaction is an essential rate-limiting step in the *de novo* biosynthesis of guanine nucleotides [6–18]. In subsequent reactions, ATP-dependent GMP synthetase (EC 6.3.5.2) catalyses the conversion of XMP to GMP, which can either be further converted into GDP and GTP or back to IMP by a two-step reaction catalysed by an NADPH-dependent guanosine 5′-monophosphate dehydrogenase (GMPR, EC 1.7.1.7). During the first step, GMP is deaminated and the covalent intermediate adduct GMPR-XMP* and $NH_3$ are formed. In the second step, the intermediate adduct is reduced to IMP by NADPH, and both reaction products ($NADP^+$ and IMP) are released from GMPR [19].

IMPDHs and GMPRs belong to the IMPDH enzyme family. The members of this family share several common structural features, including a $(\beta/\alpha)_8$ barrel structure of the catalytic domains which form a tetramer or an octamer. They also share the modes of ligand binding and the formation of a covalent enzyme–XMP* catalytic intermediate [19–21]. A structural feature characteristic of IMPDHs is the presence of cystathionine-β-synthase domains (CBSs; CBS dimers are called Bateman domains), which usually regulate enzymatic activity or multimerisation upon nucleotide binding [13,22–25]. The deletion of the IMPDH CBS in *Escherichia coli* causes the dysregulation of the adenine and guanine nucleotide pool [26,27]. So far characterised GMPRs from different

organisms, except for those described for the pathogenic protozoans *Trypanosoma brucei* (Tb GMPR) [28], *Trypanosoma congolense* (Tc GMPR) [29] and *Leishmania donovani* (Ld GMPR) [30], do not possess the CBS domain. The structural analysis of Tb GMPR has recently shown that ATP induces octamer dissociation, while guanine nucleotides do not influence the enzyme's oligomeric state [31].

Whereas IMPDH activity is strictly required for guanine nucleotide metabolism, the role of salvaging GMPR reductase activity at different bacterial life cycle stages and under stress conditions is still not well understood. GMPR is not essential for the growth of either Gram-negative bacteria such as *E. coli* [32,33] or Gram-positive species such as *Bacillus subtilis* [34], and its expression can be regulated by the intracellular ratio of adenine and guanine nucleotide pools [35,36]. The presence of an enzyme with GMPR activity in mycobacteria has not yet been identified.

Three GuaB proteins belonging to the IMPDH family are encoded in the Mtb genome (Fig. 1B). The exclusive IMPDH activity has been confirmed only for GuaB2 [16], while the GuaB1 and GuaB3 catalytic activities have not identified yet. The random saturating transposon mutagenesis of the Mtb genome has shown that the *guaB3* gene is required for the *in vitro* growth on the minimal [37] as well as on rich media [38,39] but the *guaB1* gene is dispensable. The *guaB2* and *guaB3* genes are separated by a 19-bp DNA linker in one operon unit, whereas *guaB1* is distantly located in an independent operon unit. Msm *guaB* genes have a similar genome organisation and the corresponding Mtb and Msm GuaB proteins show a homology of more than 90% (Fig. 1B). The amino acid alignment of Msm GuaB proteins shows that GuaB1 is more sequentially similar to GuaB2 (IMPDH) than to GuaB3 (Fig. 1C). While GuaB1 and GuaB2 have similar length, GuaB3 lacks the corresponding sequence of

the GuaB2 CBS domain. The majority of the amino acid residues involved in the IMP and NAD$^+$ binding in GuaB2 are not present in GuaB3, but most of them are conserved in GuaB1 (Fig. 1C). The GuaB2 active-site loop involving the catalytic Cys325 residue is conserved in GuaB1 but not in GuaB3. However, no structural data and biochemical characterisation of mycobacterial GuaB1 or GuaB3 are available yet.

This study shows that the Msm and Mtb *guaB1* genes encode an active guanosine 5′-monophosphate reductase, which is not essential for bacterial survival but contributes to the recycling of purine nucleotides. The activity of Msm GMPR is allosterically regulated by the ATP:GTP ratio only at pH values below 7, suggesting different GMPR activities in growing bacteria and during latent infection when the intracellular pH decreases [40–42]. X-ray crystallography has confirmed that Msm GMPR contains the CBS domain with an atypical position in the octamer. Phylogenetic analysis has indicated the presence of *guaB1*-encoded GMPRs with CBSs throughout the Actinobacteria phylum.

## Results

### Msm GuaB1 is an NADPH-dependent GMPR involved in the purine-salvage pathway

To investigate the potential role of GuaB1 in mycobacterial purine nucleotide biosynthesis, we knocked out the *guaB1* gene in Msm. As a control, we also knocked out the *guaB2* gene encoding IMPDH. The *ΔguaB1* Msm strain did not require any purine supplement for the growth and did not exhibit any growth defects in media containing hypoxanthine, guanine and adenine (Fig. 2A), indicating that GuaB1 is not essential for Msm growth on the synthetic 7H10/ADC agar medium. As expected, the IMPDH-null *ΔguaB2* strain exhibited guanine auxotrophy; it grew only in a medium supplemented with guanine and not in media supplemented with hypoxanthine or adenine (Fig. 2A).

Next, we blocked the *de novo* purine metabolic pathway by knocking out the essential *purF* gene, which encodes amidophosphoribosyltransferase, catalysing the first step of purine *de novo* biosynthesis (Fig. 1A), and compared the growth of the *ΔguaB1ΔpurF* strain with wt and *ΔpurF* Msm strains [43,44]. For its growth, the *ΔpurF* strain needed an external source of purine such as hypoxanthine, adenine or guanine (Fig. 2B), which serve as precursors for purine metabolism via the corresponding salvaging enzymes (Fig. 1A) [44]. The *ΔguaB1ΔpurF* strain grew on media containing adenine or hypoxanthine but not on media containing guanine as the sole purine source (Fig. 2B).

The defect of guanine utilisation in the *ΔguaB1ΔpurF* strain confirmed the involvement of Msm GuaB1 in the guanine-derived metabolite interconversion to other purines through the purine-salvage pathway. The growth of the *ΔguaB1ΔpurF* Msm strain on media supplemented with guanine was restored by complementary expression of Msm or Mtb GuaB1 from an integrated pFLAG plasmid (Fig. 2C,D), which demonstrates that both Msm and Mtb GuaB1 function within the guanine-salvage pathway.

To further biochemically characterise GuaB1, we produced recombinant Msm GuaB1 in *E. coli*. Nevertheless, because of the tendency of Mtb GuaB1 to form inclusions, we did not receive the soluble Mtb GuaB1 from this expression system. Finally, we were able to produce a low amount of Mtb GuaB1 in the Msm *ΔguaB1* strain. Therefore, we compared only the basic activities of Msm GuaB1 and Mtb GuaB1 enzymes and performed a detailed kinetics analysis only for Msm GuaB1. To avoid the loss of detected activities, we used a higher concentration of Msm and Mtb GuaB1 (500 nM) to detect the dependence on NADPH and different guanine nucleotides in the spectrophotometric assay (Fig. 2E). Importantly, we detected activity in the presence of GMP but not in the presence of the other guanine nucleotides tested with both enzymes. Chromatographic analysis of the enzymatic mixture showed the formation of IMP and NADP$^+$ (Fig. 2F). Our results have confirmed that GuaB1 (hereafter referred to as Msm GMPR) functions as a mycobacterial NADPH-dependent guanosine 5′-monophosphate dehydrogenase catalysing the reduction in GMP to IMP and ammonium with the concomitant oxidation of NADPH (Fig. 2G).

To assess the effect of *guaB1* gene deletion on purine composition, we analysed the intracellular purine metabolites in the wt and *ΔguaB1* strains during exponential growth using the fast acetic acid metabolome extraction approach in combination with hydrophilic interaction liquid chromatography (HILIC) coupled with UV/MS detection [45]. Both strains contained comparable amounts of adenine and guanine nucleotides (Fig. 3A). To evaluate the influence of *guaB1* gene deletion on Msm growth, wt, *ΔguaB1* and *ΔguaB1*pFLAG*guaB1* strains were cultivated in the 7H9/ADC medium at pH 5.5 and 6.9, mimicking macrophage intracellular pH, at which mycobacteria survive, and the pH during the replication respectively. The *ΔguaB1* strain showed the slower growth rate in the late exponential phase compared to the wt and *ΔguaB1*pFLAG*guaB1* strains at pH of 5.5. However, the delayed growth effect of the *ΔguaB1* strain was not detected at pH 6.9 (Fig. 3B). Furthermore, we compared the viability of Msm wt, *ΔguaB1* and
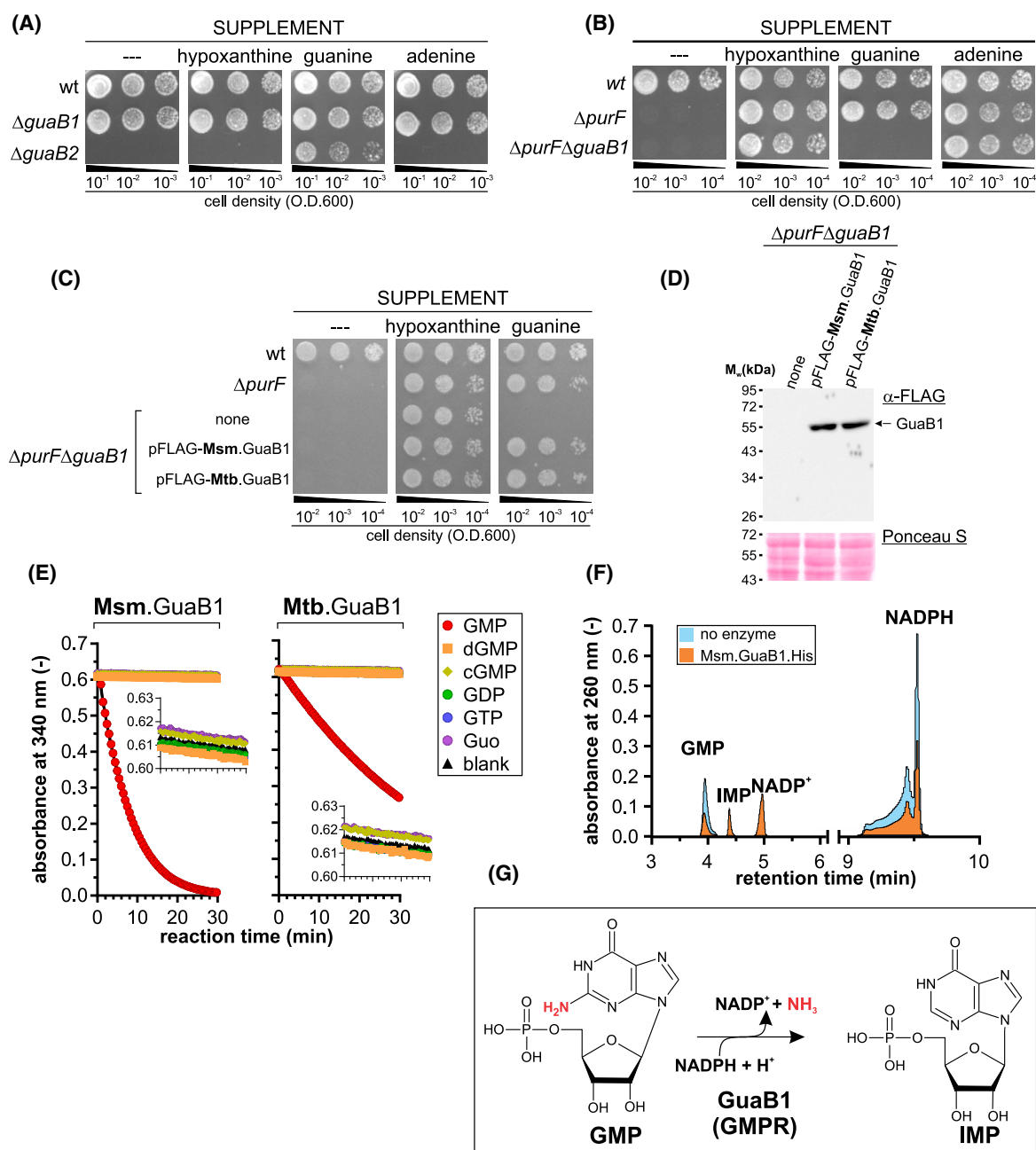
**Fig. 2.** An analysis of GuaB1 function and activity. (A) The growth of *ΔguaB1* and *ΔguaB2* strains in media supplemented with different purine nucleotides. Exponentially grown Msm strains were spotted at three O.D._600 values ($10^{-2}$, $10^{-3}$ and $10^{-4}$) on the 7H10/ADC medium with or without a 100-μM purine nucleobase supplement and incubated at 37 °C for 3 days. (B) The growth of the *ΔpurF* and *ΔguaB1ΔpurF* Msm strains under the conditions used in panel A. (C) Complementation of GuaB1 deficiency. The *ΔguaB1ΔpurF* strains, transformed with the pFLAG plasmid carrying the Msm or Mtb *guaB1* gene, were grown on the 7H10/ADC medium with or without 100 μM guanine and hypoxanthine supplementation. The wt and *ΔpurF* strains are shown as controls. (D) The immunoblot analysis of the Msm and Mtb GMPR expression in the parental *ΔguaB1ΔpurF* strain and pFLAG transformants using anti-Flag antibodies and membrane staining with Ponceau S. (E) The determination of the guanosine 5′-monophospate reductase activity of GuaB1 *in vitro*. The absorbance at 340 nm of reaction mixtures containing 500 nM recombinant Msm or Mtb GuaB1, 100 μM NADPH and 1 mM guanine nucleotides (cGMP, GMP, dGMP, GDP and GTP) or 1 mM guanosine (Guo) was continuously monitored for 30 min in MPH buffer at pH 7.8 at 25 °C. (F) An analysis of the reaction mixture with and without Msm GuaB1. Reaction mixtures containing 200 μM NADPH and 100 μM GMP without GuaB1 (light-blue field) or with 100 nM GuaB1 (orange field) were incubated for 30 min at 25 °C and analysed by UPLC on a reversed-phase column. The peaks were identified based on nucleotide calibration standards. (G) A scheme of the GMPR reaction catalysed by GuaB1.
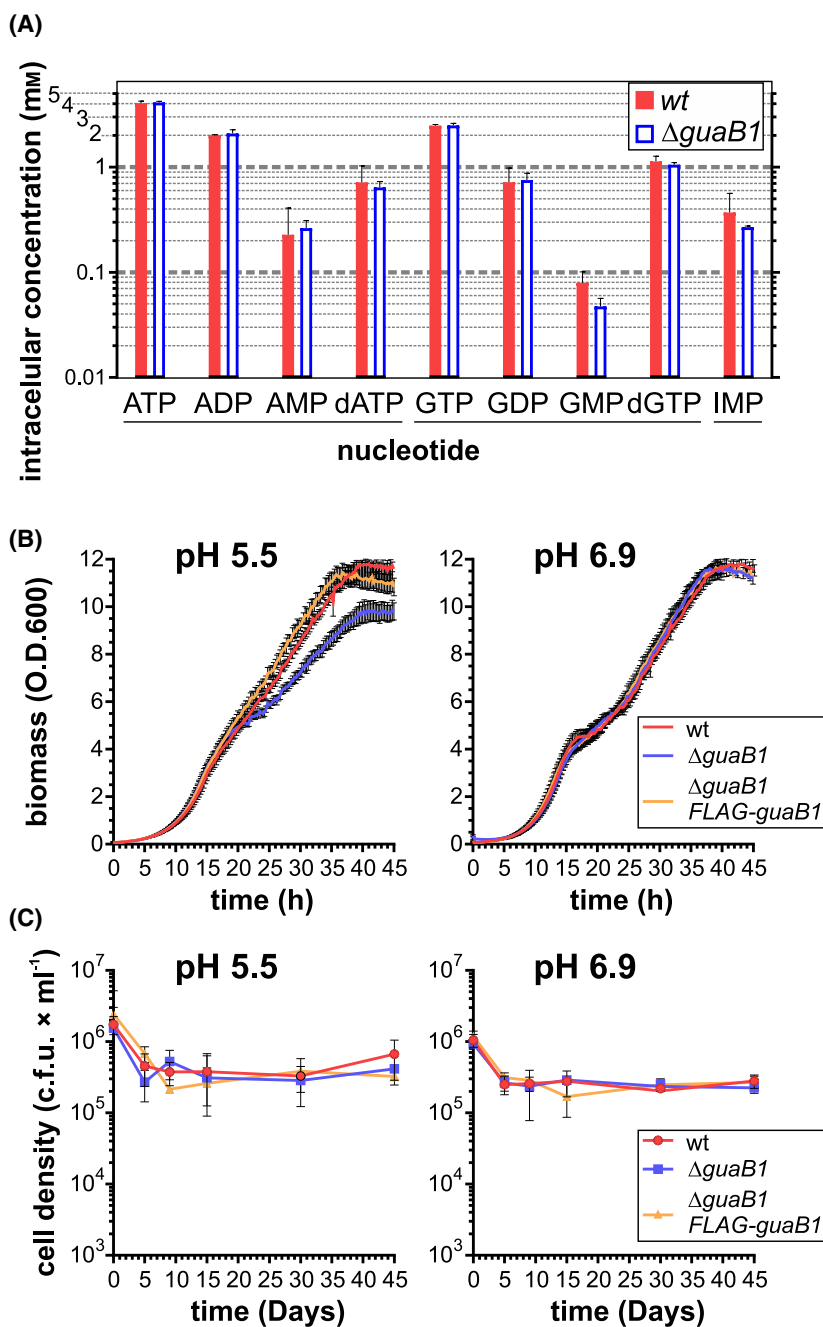
**(A)**



**(B)**



**(C)**



**Fig. 3.** Phenotypic characterisation of the *ΔguaB1* Msm strain. (A) The intracellular purine nucleotide pool in the wt and *ΔguaB1* strain. Exponentially growing cells were collected by filtration and quickly lysed with 1 M acetic acid. The extracted nucleotides were analysed by HILIC chromatography coupled with MS spectrometry and UV detection (error bars – SD, $n = 2$). (B) The wt, *ΔguaB1* and *ΔguaB1*pFLAG*guaB1* strain growth curves in the 7H9/ADC medium at pH 5.5 and 6.9. The growth was monitored by a Bioscreen instrument at 37 °C in 15-min intervals (error bars – SD, $n = 5$). (C) The wt, *ΔguaB1* and *ΔguaB1*pFLAG*guaB1* strain survivals under nutrient starvation at pH 5.5 and 6.9. The strains were grown to exponential phase, washed three times by sterile water and resuspended in phosphate buffer with corresponding pH at the starting density of approximately $10^6$ c.f.u·mL$^{-1}$. Suspensions were cultivated at 37 °C (glass tubes, magnetic stirrer, 100 r.p.m.) and viable cells at individual time points of the starvation were determined by plating on the 7H10/ADC medium (error bars – SD, $n = 2$).

*ΔguaB1*pFLAG*guaB1* strains under 45-day starvation conditions at both pH values, 5.5 and 6.9 respectively. As illustrated by Fig. 3C, GuaB1 is not dispensable for Msm adaptation to nutrient starvation and survival.

## The dependence of GMPR activity on pH and monovalent cations

We analysed Msm and Mtb GMPR activities at pH values ranging from 6.2 to 9 (Fig. 4A). The pH optima of Msm GMPR and Mtb GMPR were 7.4–7.8 and 7.6–8.2 respectively. Mtb GMPR activity was, however, significantly lower than that of Msm GMPR at all tested pH values.

Trypanosomal GMPRs require monovalent ions for catalytic activity, but the effect of individual cations on these enzymes is different [28,29]. We analysed the influence of monovalent cations on both Msm and Mtb GMPR activity and detected negligible activity in the presence of Na$^+$ and increasing activity as follows:
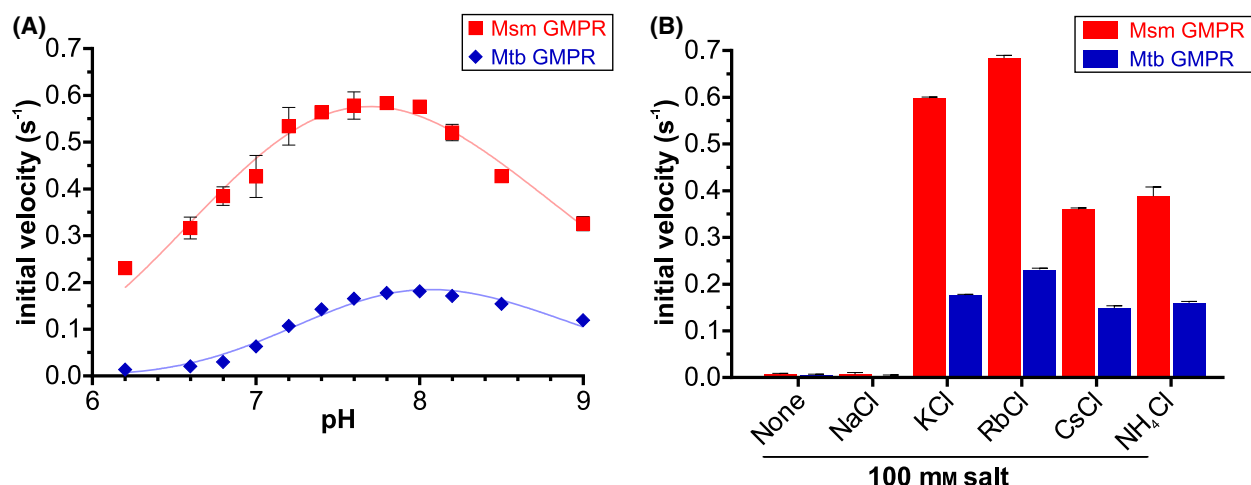
**Fig. 4.** The dependence of Msm and Mtb GMPR activities on pH and monovalent cations. (A) The determination of pH optima. Reaction velocities were measured in a mixture of 80 mM MPH buffer, 100 mM KCl and 100 nM Msm GMPR at fixed concentrations of 200 μM NADPH and 100 μM GMP as substrates (error bars – SD, $n = 3$). (B) The influence of monovalent cations on GMPR activity. Reaction velocities were measured at pH 7.8 in the presence of 100 mM of the corresponding salts, 200 μM NADPH and 100 μM GMP (error bars – SD, $n = 2$).

$Cs^+ \approx NH_4^+ < K^+ < Rb^+$ (Fig. 4B). For Msm GMPR, the initial velocities in the presence of $Rb^+$ and $K^+$ were $0.68 \pm 0.02$ $s^{-1}$ and $0.60 \pm 0.01$ $s^{-1}$ respectively. The reaction velocities in the presence of $Cs^+$ and $NH_4^+$ were reduced by approximately 40% to $0.36 \pm 0.01$ $s^{-1}$ and $0.39 \pm 0.03$ $s^{-1}$ respectively. Mtb GMPR exhibited similar activity dependence on monovalent ions.

## GMPR activity is regulated by substrates and reaction products

Next, we measured the kinetic parameters of Msm and Mtb GMPR near their pH optima (pH 7.8). The plot of the initial reaction velocity as a function of NADPH concentration at a fixed GMP concentration (100 μM) followed Michaelis–Menten kinetics for Msm and Mtb GMPRs (Fig. 5A). The apparent Michaelis–Menten constant ($K_m$) values for NADPH were $30 \pm 4$ μM and $63 \pm 7$ μM for Msm and Mtb GMPR respectively. The corresponding apparent limiting initial velocities were calculated as $0.73 \pm 0.03$ $s^{-1}$ (Msm) and $0.27 \pm 0.08$ $s^{-1}$ (Mtb). The catalytic efficiency value ($k_{cat}/K_m$) of Mtb GMPR was six times lower when compared to its Msm counterpart (Table 1).

On the other hand, the plot of the initial reaction velocity versus GMP concentration at a fixed NADPH concentration (200 μM) for both Msm and Mtb GMPR showed rather negative cooperativity, unlike the Michaelis–Menten dependence (Fig. 5B). The Hill coefficient ($n_H$) was calculated as

$0.53 \pm 0.05$ and $0.52 \pm 0.03$ for Msm and Mtb GMPR respectively. The apparent $K_{0.5}$ values for GMP were $4.2 \pm 0.6$ μM for Msm GMPR and $10.5 \pm 1.17$ μM for Mtb GMPR. The apparent Msm GMPR $V_{lim}$ value was approximately five times higher in comparison with Mtb GMPR. Reaction products and substrate analogues often inhibit enzymatic reactions. Therefore, we evaluated Msm GMPR activity in the presence of IMP (product) and XMP (reaction intermediate). Our analysis showed that IMP (Fig. 5C) and XMP (Fig. 5D) are competitive inhibitors of Msm GMPR with $K_i$ values of $10 \pm 0.4$ μM and $0.6 \pm 0.1$ μM respectively.

The Msm and Mtb GMPR pH optima are approximately 1 unit higher in comparison with the intracellular pH of mycobacteria, which ranges between 6.5 and 7.2 in dependence on the bacterial physiological state and extracellular conditions [40–42]. At slightly acidic pH (6.6), we were able to determine kinetic parameters only for Msm GMPR but not for Mtb GMPR due to its low measurable activity (Fig. 4A). The apparent Michaelis–Menten constant ($K_m$) and apparent limiting initial velocity values for NADPH at pH 6.6 were $63 \pm 4$ μM and $0.51 \pm 0.01$ μM respectively. Msm GMPR showed approximately three times lower catalytic efficiency at pH 6.6 in comparison with the optimal pH 7.8 (Table 1). The initial velocity *versus* GMP concentration plot for Msm GMPR still showed negative Hill cooperative dependence at pH 6.6 (Table 1). The $K_{0.5}$ GMP values at pH 6.6 and 7.8 were comparable (Table 1).
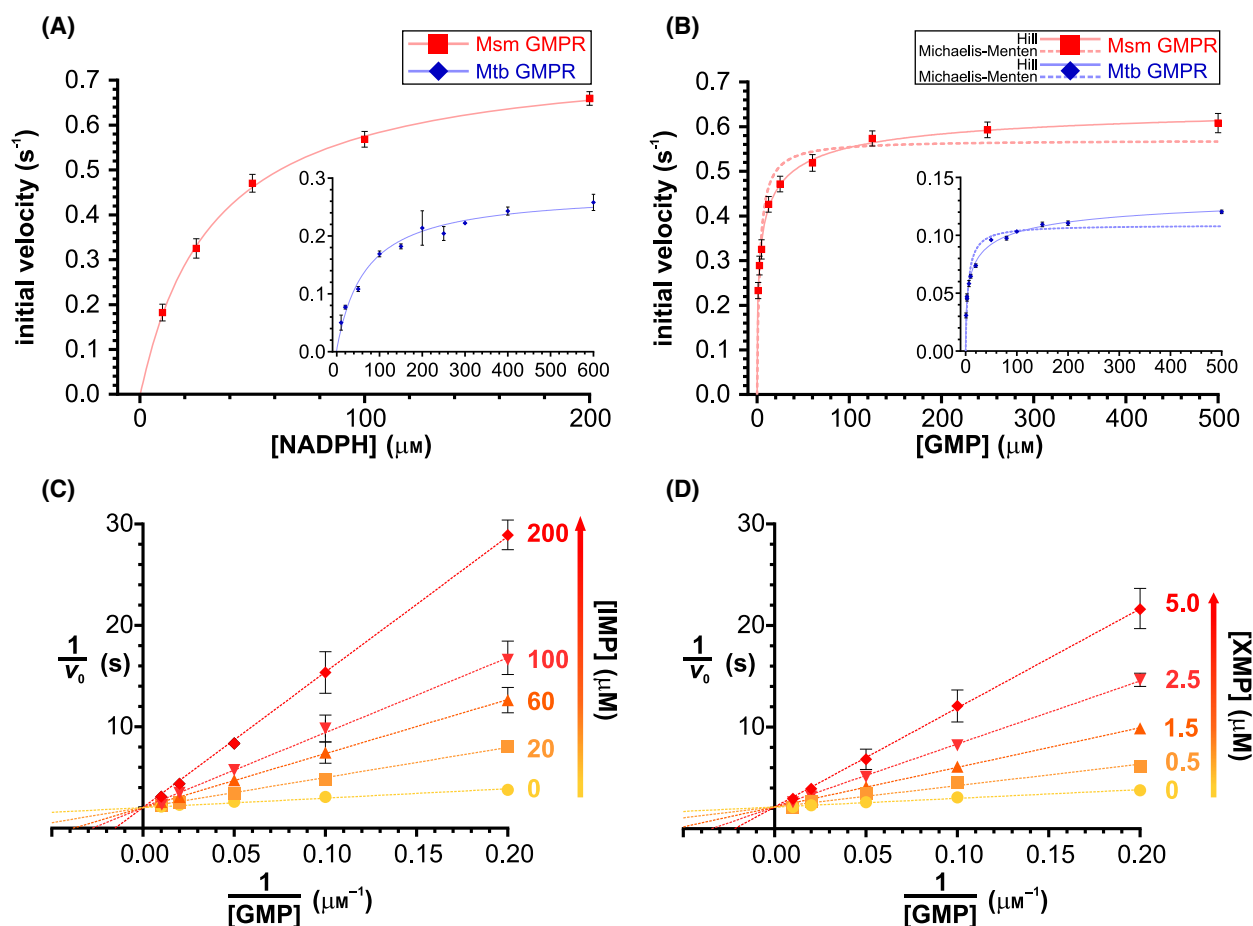
**Fig. 5.** The steady-state kinetics of the Msm and Mtb GMPR-catalysed reaction at pH 7.8. Reaction velocities were measured in 80 mM MPH buffer, 100 mM KCl and 20 nM Msm GMPR and 40 nM Mtb GMPR, respectively, at pH 7.8 and 25 °C. (A) The dependence of the initial reaction velocity on the NADPH concentration at a fixed GMP concentration (100 μM). The data were fitted with the Michaelis–Menten equation. The inner insert is a graph for Mtb GMPR (error bars – SD, $n = 2$). (B) The dependence of the initial reaction velocity on the GMP concentration at a fixed NADPH concentration (200 μM). The data were fitted with the Hill (solid line) or Michaelis–Menten (dotted line) equation. The inner insert is a graph for Mtb GMPR (error bars – SD, $n = 3$). (C) The inhibition of Msm GMPR activity by IMP shown in Lineweaver–Burk representation. The IMP concentration is shown to the right of each line (error bars – SD, $n = 2$). (D) The inhibition of Msm GMPR activity by XMP shown in Lineweaver–Burk representation. The XMP concentration is shown to the right of each line (error bars – SD, $n = 2$).

## Msm GMPR activity is inhibited by ATP in a pH-dependent manner

We tested the effect of a physiologically relevant 1 mM ATP or GTP on Msm GMPR activity in the presence of 2 mM MgCl$_2$ at fixed substrate concentrations 100 μM GMP and 200 μM NADPH. At pH 7.8, GTP had only a minor positive effect and ATP only a minor negative effect on the activity. At lower pH values, however, the effects of ATP and GTP increased (Fig. 6A). The inhibitory effect of 1 mM ATP increased sigmoidally with decreasing pH (7.8–6.4), plateauing at pH 6.6. In contrast, the activating effect of 1 mM GTP increased linearly with decreasing pH.

In order to analyse the impact of GTP and ATP on GMPR activity at pH 6.6 more deeply, we measured the initial velocity of the reactions in the absence or presence of these nucleotides *versus* GMP concentration (Fig. 6B, Table 1). At 1 mM concentrations, GTP and ATP caused only minor changes to $n_H$ and $K_{0.5}$. The $n_H$ value changed from $0.67 \pm 0.04$ to $0.65 \pm 0.06$ and $1.29 \pm 0.18$, respectively, and the $K_{0.5}$ value changed from $2.7 \pm 0.3$ to $3.5 \pm 0.3$ and $1.9 \pm 0.1$ μM respectively. However, the changes to $V_{lim}$ were more substantial. The addition of 1 mM GTP increased the $V_{lim}$ from $0.39 \pm 0.01$ to $0.51 \pm 0.01$ s$^{-1}$ (a 36% increase), whereas the addition of 1 mM ATP decreased $V_{lim}$ to $0.056 \pm 0.001$ s$^{-1}$ (an 86% decrease).

**Table 1.** The basic kinetic parameters of reactions catalysed by Msm and Mtb GMPR under different conditions.

| Species | pH | Ligand | Varied substrate | $V_{\text{lim}}^{\text{app}}$ s$^{-1}$ ± SD | $K_{\text{m}}^{\text{app}}$ ($K_{0.5}^{\text{app}}$) {M ± SD | Dependence | $k_{\text{cat}}/K_{\text{m}}$ {M$^{-1}$·s$^{-1}$ |
|---|---|---|---|---|---|---|---|
| Msm | 7.8 |  | NADPH | 0.73 ± 0.03 | 30 ± 4 | MM eq. | 0.024 |
| Msm | 7.8 |  | GMP | 0.66 ± 0.02 | 4.2 ± 0.6 | Hill eq. $n_{\text{H}}$ 0.53 ± 0.05 |  |
| Msm | 6.6 |  | NADPH | 0.51 ± 0.01 | 63 ± 4 | MM eq | 0.008 |
| Msm | 6.6 |  | GMP | 0.39 ± 0.01 | 3.5 ± 0.3 | Hill eq. $n_{\text{H}}$ 0.67 ± 0.04 |  |
| Msm | 6.6 | 1 mM GTP | GMP | 0.51 ± 0.01 | 2.7 ± 0.3 | Hill eq. $n_{\text{H}}$ 0.65 ± 0.06 |  |
| Msm | 6.6 | 1 mM ATP | GMP | 0.056 ± 0.001 | 1.9 ± 0.1 | Hill eq. $n_{\text{H}}$ 1.29 ± 0.18 |  |
| Mtb | 7.8 |  | NADPH | 0.27 ± 0.08 | 63 ± 7 | MM eq. | 0.004 |
| Mtb | 7.8 |  | GMP | 0.13 ± 0.01 | 10.5 ± 1.17 | Hill eq. $n_{\text{H}}$ 0.52 ± 0.03 |  |
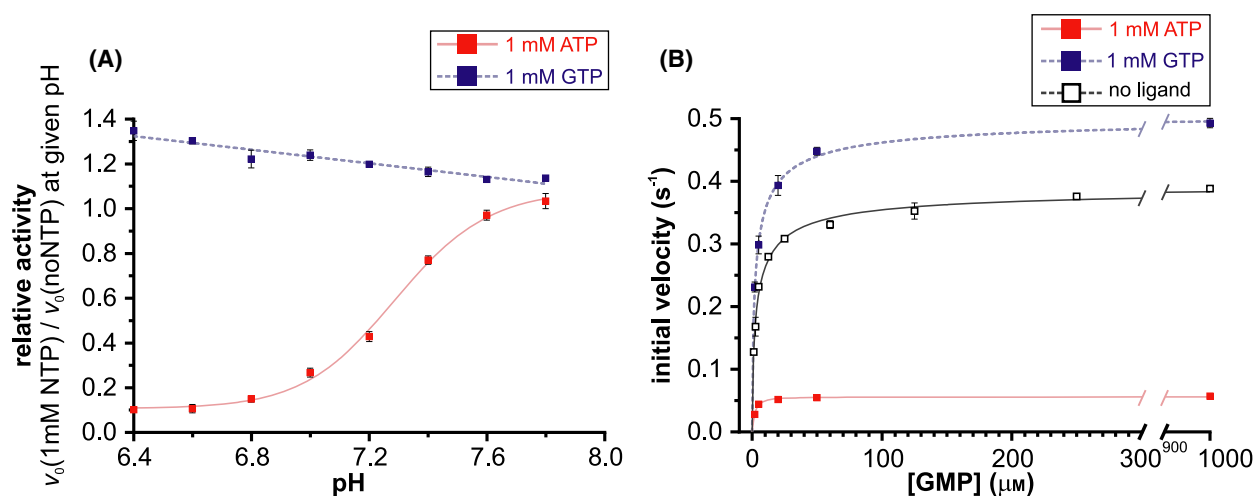


**Fig. 6.** The influence of ATP and GTP on Msm GMPR activity. (A) The dependence of the relative Msm GMPR activity on pH in the presence of 1 mM ATP or GTP. The relative activity is the ratio of the initial velocity of the reaction with 1 mM NTP and the velocity of the control reaction without NTPs. For ATP and GTP, the data were fitted with Hill and linear equations respectively. All reactions were performed at fixed substrate concentrations (100 μM GMP and 200 μM NADPH), 2 mM MgCl$_2$ and 100 nM Msm GMPR in 80 mM MPH buffer at 25 °C (error bars – SD, $n$ = 2). (B) The plots of the initial velocity *versus* GMP concentration in the presence of or without a ligand and 1 mM GTP and 1 mM ATP at pH 6.6. All reactions were performed at fixed NADPH concentrations (200 μM) and 30 nM Msm GMPR in 80 mM MPH buffer containing 2 mM MgCl$_2$ at 25 °C (error bars – SD, $n$ = 2).

## ATP-dependent Msm GMPR inhibition is restored by increasing GTP concentration

In our experimental setup, Msm GMPR activity is negatively regulated by 1 mM ATP but positively regulated by 1 mM GTP at slightly acidic pH. *In vivo*, however, both ATP and GTP, the endpoint products of the purine metabolic pathway, can concurrently affect Msm GMPR activity. The relative Msm GMPR activity sigmoidally decreased with increasing ATP concentration and the IC$_{50}$ value calculated for ATP was 57 ± 1 μM at pH 6.6 (Fig. 7A). Therefore, we

measured Msm GMPR activity in the presence of 57 μM ATP or 570 μM ATP (10 × IC$_{50}$) at increasing GTP concentrations (Fig. 7B). At both ATP concentrations, the activity increased sigmoidally from the most inhibited to fully recovered. In the presence of 57 μM ATP, half of the activity was recovered at 27 ± 2 μM GTP. In the presence of 570 μM ATP, half of the Msm GMPR activity was recovered at 470 ± 11 μM GTP. These results indicate that the activity of Msm GMPR can be tightly regulated by the ATP/GTP ratio.
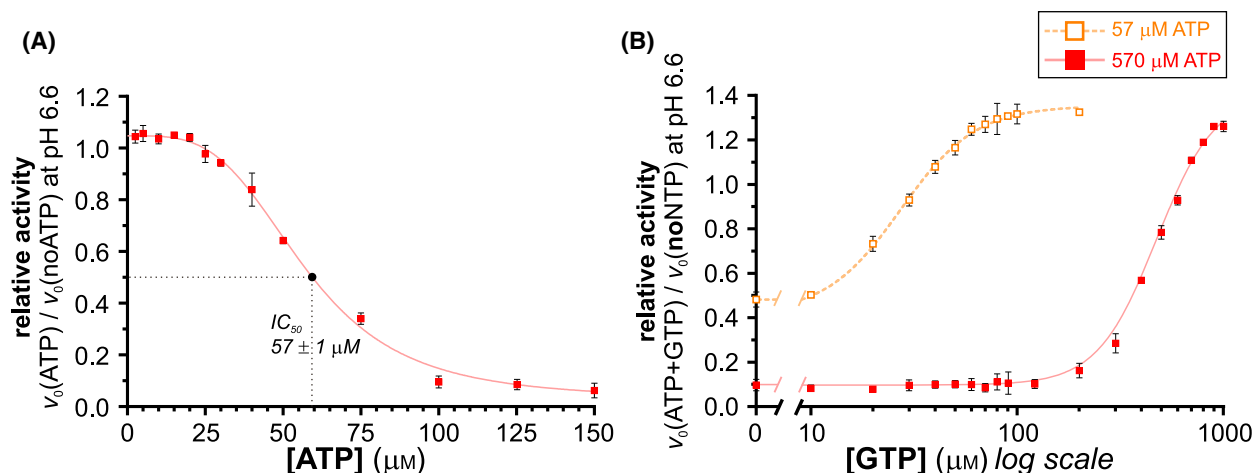
**Fig. 7.** Msm GMPR inhibition by ATP and the restoration of its activity by GTP. All reactions were performed at fixed substrate concentrations (100 μM GMP and 200 μM NADPH), 2 mM MgCl$_2$ and 100 nM Msm GMPR in 80 mM MPH buffer at 25 °C, (A) The dependence of the relative Msm GMPR activity on ATP concentration at pH 6.6. The relative activity is the ratio of the reaction velocity at the given ATP concentration and the velocity of the reaction without ATP. The data were fitted with the Hill equation (error bars – SD, $n = 2$). (B) The effect of GTP on Msm GMPR activity inhibited by ATP. The activity of Msm GMPR at increasing concentrations of GTP was measured in the presence of 57 μM ATP (orange open squares) or 570 μM ATP (red filled squares). The relative activity is the ratio of the initial reaction velocities measured in the presence and absence of ATP and GTP (error bars – SD, $n = 2$).

## The oligomerisation state of Msm GMPR is regulated by ligands and pH

In order to determine whether the oligomerisation state of Msm GMPR is regulated by nucleotide binding, we used size-exclusion chromatography to analyse Msm GMPR in the presence of GMP, IMP, GTP and ATP at various pH values (6.6, 7.3 and 8.2). The oligomeric state of the protein was then expressed as the percentage of protein-forming tetramers (Fig. 8). In all experiments, we observed only tetramers or octamers.

The apo forms of Msm GMPR and Msm GMPR with GTP were present only as octamers at all the pH values tested. Nevertheless, Msm GMPR with GMP, IMP or ATP formed octamers and tetramers in a pH-dependent manner; the higher the pH, the stronger the effect of the ligands on the dissociation of the octamers. At pH 8.2, 33–59% of the protein formed tetramers. At pH 7.3, 15–21% of the protein formed tetramers. At pH 6.6, the effect of the ligands was not observable. This indicates that pH plays an important role in the dissociation of Msm GMPR octamers to tetramers in the presence of a substrate (GMP), product (IMP) or activity effector (ATP).

Subsequently, we analysed the effect of GTP or ATP on the oligomeric state of the GMPR:GMP complex. Interestingly, both ligands induced octamerisation of the complex. At pH 8.2, the percentage of Msm GMPR-forming tetramers decreased from 52% to 8% in the presence of GTP and to 14% in the

presence of ATP. At pH 7.3 and 6.6, no tetramers were observed.

## X-ray crystallography shows the unique position of CBS domains in the Msm GMPR octamer

The structure of *T. brucei* GMPR is the only known structure of GMPR that contains CBS domains [31]. The presence of CBS domains in GMPRs is unusual. However, an analysis of the Msm GMPR amino acid sequence and its alignment with sequence of Msm IMPDH have shown that residues Arg92–Arg214 in Msm GMPR are located at the position corresponding to the IMPDH CBS (region Glu110–Arg236, Fig. 1C). To confirm the presence of a CBS domain in Msm GMPR and to learn how the structure of Msm GMPR differs from the structures of other IMPDHs and GMPRs, we determined the structure of Msm GMPR by X-ray crystallography.

Msm GMPR readily crystallised in many different screened conditions. However, even after extensive optimisation, most of the crystals were of low quality and contained various pathologies that usually prevented successful molecular replacement or structure refinement. The protein crystallised in several space groups (P1, P2$_1$, C2 and P2$_1$2$_1$) and, interestingly, sometimes even in the same drop. The final crystals of the Msm GMPR apo form were grown in a hanging drop containing 17 mg·mL$^{-1}$ Msm GMPR, 0.03 M MgCl$_2$,
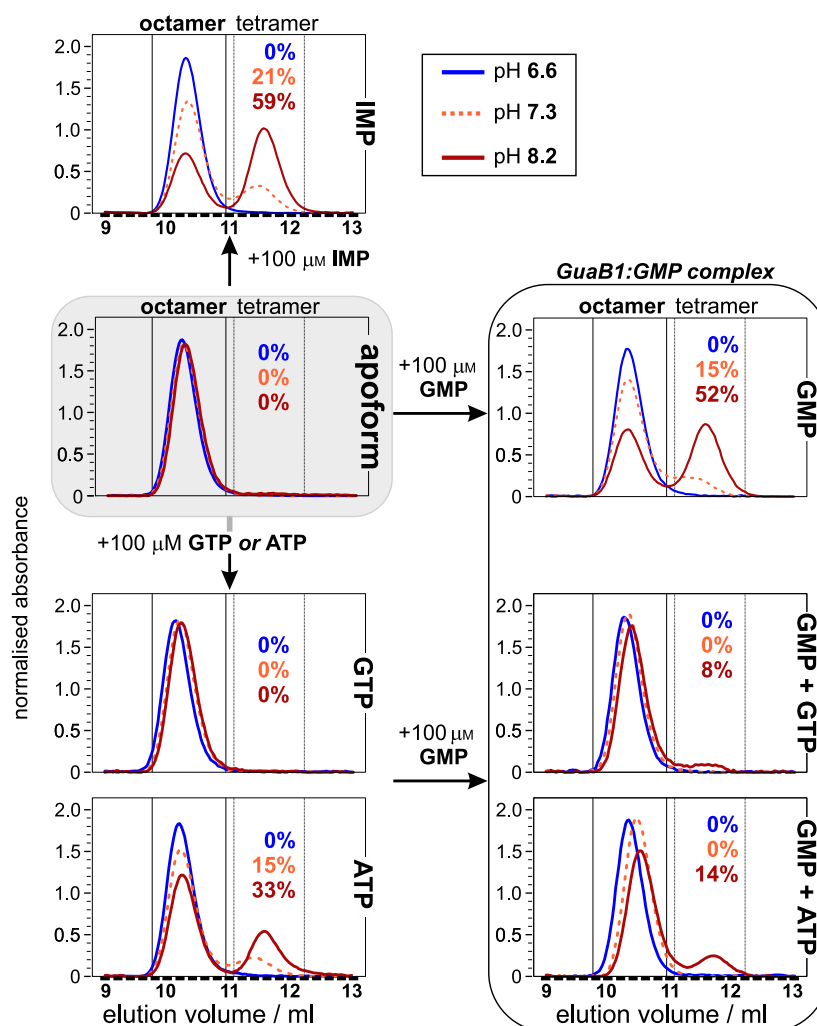
**Fig. 8.** An analysis of Msm GMPR oligomerisation. Msm GMPR (50 μM) was analysed by size-exclusion chromatography in the absence (apo form) or presence of 100 μM ligands at pH 6.6, 7.3 and 8.2. The oligomeric state of the protein is expressed as the percentage of protein-forming tetramers.

0.03 M CaCl$_2$, 20% ethylene glycol, 13% PEG 8000 and 0.1 M Tris/bicine, pH 8.5. These crystals had the space group C2 and eight monomers in the asymmetric unit. Datasets from three crystals were merged to obtain the final dataset. The final crystal of Msm GMPR in a complex with GMP was grown in a sitting drop containing 22 mg·mL$^{-1}$ Msm GMPR, 2 mM GMP, 0.2 M NaCl, 20% PEG 3000 and 0.1 M HEPES, pH 7.5. This crystal had the space group P1 and 16 monomers in the asymmetric unit. The crystal parameters and refinement statistics are listed in Table 2. The structures of the Msm GMPR apo form and its complex with GMP have been deposited in the Protein Data Bank under PDB ID 7OY9 and 7R50 respectively.

As expected, the Msm GMPR monomer is composed of two domains (Fig. 9). The catalytic domain has a TIM barrel structure typical of the IMPDH/GMPR structural family. The Msm GMPR sequence spanning residues 97–207 folds as a typical Bateman domain composed of two CBS domains. The Msm GMPR catalytic domains form a tetramer with a four-fold axis and the Bateman domains at the perimeter. Two tetramers interact through the Bateman domains, thus forming an octamer typical of IMPDHs and GPMRs with Bateman domains (Fig. 10A,B). Nevertheless, unlike Tb GMPR and all known structures of IMPDH and GPMR octamers, in which the Bateman domains protrude from the octamer and thus have few contacts with the catalytic domains (Fig. 10C,D), the Bateman domains in Msm GMPR are very close to the catalytic domains and have a relatively large interacting area.

The Bateman domains from opposing tetramers usually interact through both CBS domains, thus forming a dimer with a specific conformation (Fig. 11A). This conformation does not change even if the octamer itself is extended, compressed or twisted after nucleotide binding [31,47]. The independent movement of the

**Table 2.** Data collection and refinement statistics. Values for the highest-resolution shell are shown in parenthesis.

| | Msm GMPR apo form | Msm GMPR with GMP |
|---|---|---|
| PDB ID | 7OY9 | 7R50 |
| Data collection | | |
| Space group | C2 | P1 |
| Unit cell | | |
| *a, b, c* (Å) | 253.06, 109.83, 200.82 | 104.79, 105.10, 170.47 |
| α, β, γ (°) | 90.00, 119.43, 90.00 | 76.92, 81.86, 69.01 |
| Wavelength (Å) | 0.9184 | 0.9184 |
| Resolution range (Å) | 43.73–2.8 (2.9–2.8) | 47.69–2.5 (2.589–2.5) |
| Total reflections | 4 685 585 (479 648) | 437 781 (44 936) |
| Unique reflections | 118 145 (11 722) | 208 443 (21 247) |
| Multiplicity | 39.7 (40.9) | 2.1 (2.1) |
| Completeness (%) | 99.89 (99.94) | 90.06 (86.46) |
| *R*-merge | 0.1555 (3.968) | 0.1364 (1.632) |
| *R*-meas | 0.1575 (4.018) | 0.185 (2.22) |
| Average $I/\sigma(I)$ | 17.77 (1.07) | 5.27 (0.58) |
| Wilson *B*-factor (Å$^2$) | 94.66 | 48.86 |
| CC1/2 | 1 (0.662) | 0.992 (0.293) |
| CC* | 1 (0.892) | 0.998 (0.673) |
| Refinement | | |
| Resolution range (Å) | 43.73–2.8 (2.9–2.8) | 47.69–2.5 (2.589–2.5) |
| Reflections used in refinement | 118 056 (11 718) | 205 619 (19 716) |
| *R*-work | 0.2410 (0.4045) | 0.2635 (0.3813) |
| *R*-free | 0.2791 (0.4468) | 0.3058 (0.4325) |
| RMSD bond length (Å) | 0.010 | 0.005 |
| RMSD angle (°) | 1.25 | 1.12 |
| Atoms in AU | 25 837 | 53 060 |
| Protein atoms in AU | 25 837 | 52 676 |
| Ligand atoms in AU | 0 | 384 |
| Protein residues in AU | 3647 | 7307 |
| Average *B*-factor (Å$^2$) | 114.34 | 57.98 |
| Ramachandran favoured (%) | 98.42 | 97.03 |
| Ramachandran allowed (%) | 1.58 | 2.97 |
| Ramachandran outliers (%) | 0 | 0 |
| Rotamer outliers (%) | 1.43 | 0.50 |
| Clashscore | 5.28 | 4.91 |

dimer is enabled by the flexible linker between the catalytic and Bateman domains. However, the formation of this dimer is impossible for Msm GMPR without a substantial change in the mutual orientation of the catalytic and Bateman domains, which seems to be fixed in this protein due to the lack of a flexible linker. The mutual orientation of the interacting Bateman domains in the Msm GMPR octamer is thus unique among IMPDHs and GPMRs (Fig. 11B). Furthermore, the mutual orientation of two tetramers and, consequently, the mutual orientation of interacting Bateman domains in Msm GMPR with GMP (conformation A) differ from that in the Msm GMPR apo form (conformation B) (Figs 10A,B and 11B). However, we have no reason to believe that this conformational change is caused by GMP binding because we have obtained structures of the Msm GMPR apo form and Msm GMPR with GMP in both conformations. Unfortunately, because of the low quality of the obtained crystals, we have refined and deposited only the two above-mentioned structures. The conformation of the dimer of the Bateman domains in Msm GMPR conformation A is somewhat similar to the conformation of the dimer in known structures of other IMPDHs and GPMRs (Fig. 11). Nevertheless, the conformation of the dimer of the Bateman domains in Msm GMPR conformation B is completely different. Because of the relatively large rotation, it occurs at the very opposite sides of the Bateman domains and is much smaller (Fig. 11). At first, we thought that the different mutual orientation of the tetramers in the octamer is caused by the pH in the crystallisation conditions, but the collection of more datasets has shown that it does not correlate with the pH or any other known factor in the crystallisation conditions. The only correlation was observed between the orientation and the space group of the crystal. All crystals with the space group P1 or P2$_1$2$_1$ contained protein in conformation A, and all crystals with the space group P2$_1$ or C2 contained protein in conformation B.

Despite all these differences, the tertiary structures of the catalytic and Bateman domains in Msm GMPR do not differ from the known structures of IMPDHs and GPMRs (Fig. 12). In the structure of Msm GMPR with GMP, we found GMP bound only at the active site, unlike in Tb GMPR, where GMP was bound at the active site and the allosteric regulatory site [31]. The orientation of GMP at the active site is virtually identical to other structures of IMPDHs and GPMRs despite the differences in amino acid sequences. The interaction of GMP and the active site involves 13 hydrogen bonds. The loop that covers the active site and is usually disordered without a bound substrate is stabilised by the interaction with GMP (Fig. 13), namely by the interaction of residues Met387, Ala388, Arg391 and Glu413.
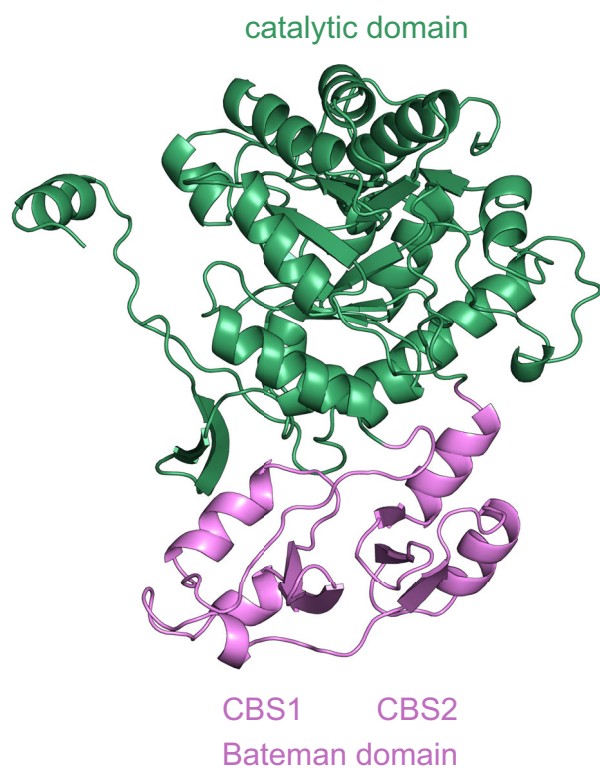
## catalytic domain

## CBS1    CBS2
## Bateman domain

**Fig. 9.** The structure of the Msm GMPR monomer determined by X-ray crystallography. The Msm GMPR monomer is composed of a catalytic domain with the TIM barrel structure typical of the IMPDH/GMPR family (green) and a Bateman domain composed of two CBS domains (pink). The structure figures were generated by using PYMOL.

### The CBS domain is necessary for Msm GMPR function *in vivo*

To test the importance of the CBS domain for GMPR function in Msm, we complemented the guanine utilisation-deficient Msm *ΔguaB1ΔpurF* strain with plasmids encoding the C-terminal FLAG-tag fused Msm GMPR or with two deletion Msm GMPR variants lacking the CBS domain, designated as S-ΔCBS (the region Arg92–Arg214 replaced by a GG motif) and L-ΔCBS (the region Val96–Leu194 replaced by an SGG motif).

Restored *ΔguaB1ΔpurF* growth on guanine as a sole purine supplement has only been observed in the presence of full-length Msm GMPR (Fig. 14A). An immunoblot analysis has shown that the expression of all three FLAG-fused GMPR variants is comparable (Fig. 14B). These results illustrate the indispensability of the CBS domain for the function of Msm GMPR. Although we have prepared several constructs and used different purification procedures, we have not succeeded in purifying the ΔCBSGMPR mutants for complementary biochemical studies.

### The Msm *guaB1* gene is an Actinobacteria phylum-specific feature

In order to determine whether GMPRs containing CBS-domain homologues (GuaB1) are also present in other organisms, we have searched for protein sequences homologous to Msm GMPR in bacterial genomes using BLAST. Our analysis has revealed GuaB1 homologues throughout the entire phylum of Actinobacteria (Fig. 15A). Genomes of Actinobacteria species contain two GuaB1 homologues with CBS domains. These GuaB1 sequence homologues typically contain two CBS domains inserted into a highly conserved IMPDH domain. Because of the principal sequence similarity between GMPRs and IMPDHs, we used the hidden Markov model (HMM) approach to confirm the identity of GuaB1 (Fig. 15B). Genes for IMPDH in Actinobacteria are accompanied by another IMPDH homologue, designated as GuaB3 in mycobacteria (Rv3410c in Mtb and MSMEG_1603 in Msm; see Fig. 1B).

## Discussion

The Msm and Mtb genomes contain three *guaB* genes each (Fig. 1B). Most studies have focused on Mtb *guaB2*, which encodes an essential IMPDH and is a potential drug target [7,14–16]. Two other genes, Mtb *guaB1* (Rv1843c) and *guaB3* (Rv3410c), and their Msm orthologues, Msm *guaB1* (MSMEG_1602) and *guaB3* (MSMEG_1603), have an unknown function and are currently annotated in databases as members of the IMPDH family.

The characterisation of mutated Msm strains lacking *guaB1* and the essential *purF* gene from the *de novo* biosynthesis pathway has shown that Msm GuaB1 is involved in guanine interconversion in the purine-salvage pathway. The testing of the *in vitro* activity and the identification of reaction products using UPLC chromatography has revealed that GuaB1 catalyses the NADPH-dependent conversion of GMP to IMP and thus serves as a guanosine 5′-monophosphate reductase. The results of positive complementation tests in the Msm *ΔguaB1ΔpurF* strain with Msm and Mtb *guaB1* sequences, the high amino acid sequence similarity of Msm and Mtb *guaB1*-encoded proteins and the testing of recombinant Msm and Mtb GuaB1 activities have demonstrated that *guaB1* encodes a GMPR in both Msm and Mtb. Our experiments have indicated that GMPR activity is not required for a long-term Msm
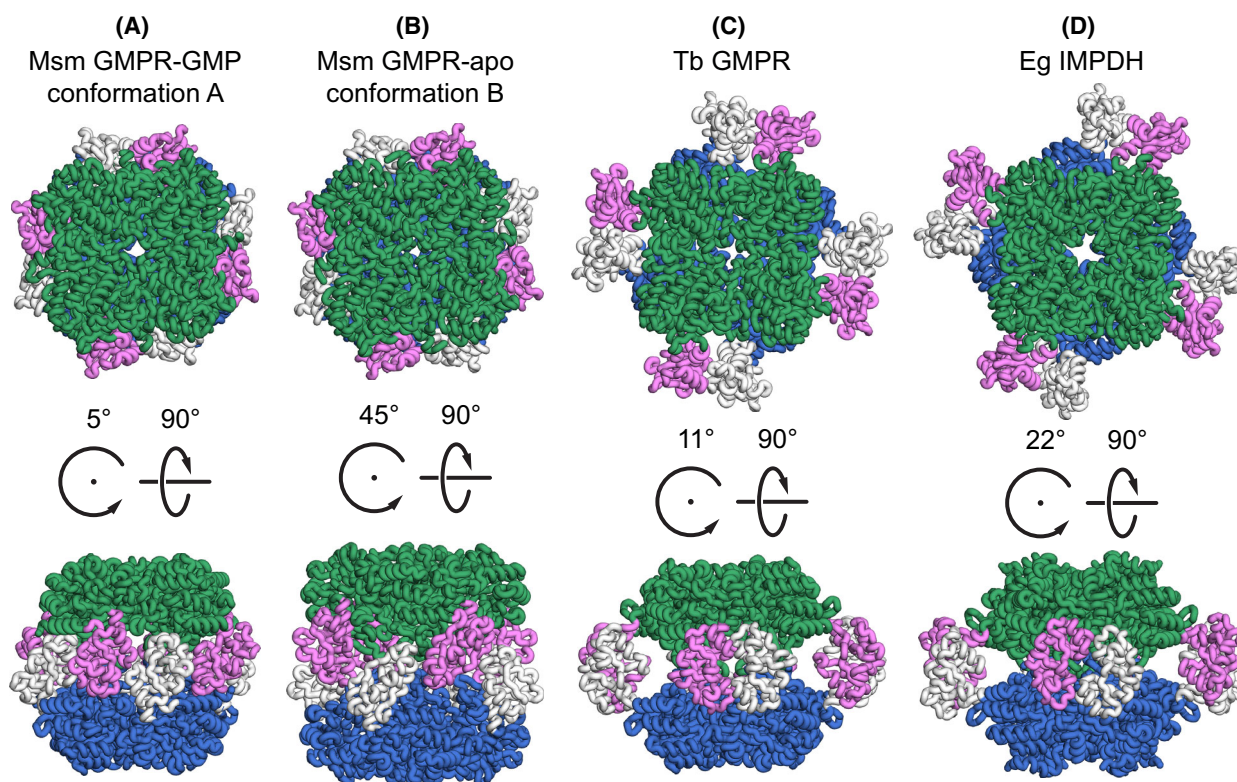
**Fig. 10.** A comparison of the quaternary organisation of Msm GMPR and the complex of Msm GMPR with GMP with *Trypanosoma brucei* (Tb) GMPR and *Eremothecium gossypii* (Eg) IMPDH. The catalytic domains (green/blue) form a tetramer with fourfold symmetry and the CBS domains (pink/white) at the perimeter. Two tetramers then form an octamer. The side views have been rotated to centre the interacting CBS domains. (A, B) The CBS domains in the Msm GMPR octamer are much closer to the catalytic domains than in the other known structures of GMPRs and IMPDHs, such as (C) the Tb GMPR apo form (PDB ID: 6JL8) [31] and (D) Eg IMPDH with bound GDP and GMP (PDB ID: 4Z87) [46]. Msm GMPR tetramers (A, B) can adopt two different mutual orientations and thus form two different dimers of the Bateman domains (see Fig. 11 for details). The structure figures were generated by using PYMOL.

adaptation to nutritional stress. On the other hand, the abolition of GMPR activity is linked with the slower growth of Msm in the late exponential phase at pH 5.5 but not at pH 6.9. Our results are consistent with previous observations about GMPR inessentiality in other bacterial species such as Mtb [38], *E. coli* [32,48], *B. subtilis* [49], *Helicobacter pylori* [50] and *Streptococcus pyogenes* [51]. On the other hand, GMPR is present across most bacterial species. This evolutionary conservation implies some benefit of the GMPR reaction for the bacterial life cycle, but further studies, such as the large-scale condition phenotypic profiling of the GMPR-null Msm strain and/or the identification of the corresponding synthetic lethal gene pair(s), might explain the GMPR importance for the mycobacterial life cycle.

Our results indicate that the properties of mycobacterial GMPRs are significantly different from the hitherto known GMPRs. Whereas Msm and Mtb GMPRs require alkali metal ions with the ionic radius of $K^+$ or higher ($Rb^+$, $Cs^+$) for catalysis, the majority of

characterised GMPRs (*Homo sapiens*, *Salmonella typhimurium*, *E. coli* and *Mycoplasma mycoides*) do not need monovalent cations for their activities [35,52–55]. Protozoal Tb GMPR and Tc GMPR exhibit increased activity in the presence of $K^+$ and $NH_4^+$ [28,29], but the essentiality of ions for GMPR activity has not been demonstrated. The requirement of monovalent cations for activity is, however, considered to be a characteristic feature of IMPDHs [56–60]. Therefore, to the best of our knowledge, mycobacterial GMPRs are the first GMPRs to be identified as strictly requiring monovalent ions for activity.

Another unique feature of Msm and Mtb GMPRs is the presence of a CBS sequence motif, spanning the amino acid residues 97–207, which forms the Bateman domain. So far, only protozoal GMPRs are known to harbour the CBS domain [30,31]. The presence of the CBS domain is very likely to contribute also to different kinetic properties of mycobacterial GMPRs. The hitherto characterised GMPRs lacking the CBS
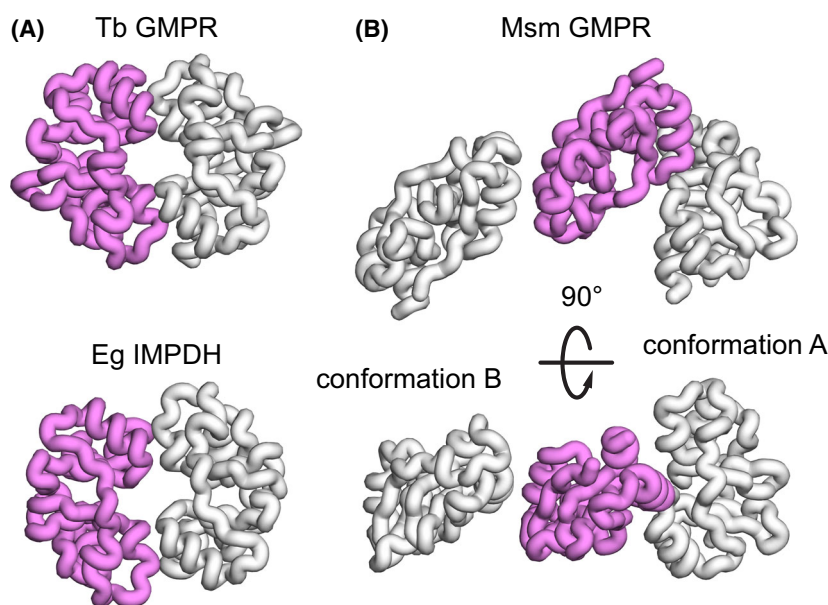
**Fig. 11.** The dimer interface of the Bateman domains in Msm GMPR and its comparison to the Bateman domains of *Trypanosoma brucei* (Tb) GMPR and *Eremothecium gossypii* (Eg) IMPDH. (A) The dimers of the Bateman domains typical of GMPRs and IMPDHs, such as the Tb GMPR apo form (PDB ID: 6JL8) [31] and Eg IMPDH with bound GDP and GMP (PDB ID: 4Z87) [46]. Msm GMPR Bateman domains cannot form this dimer because they cannot rotate independently of the catalytic domains. (B) Msm GMPR has formed two different dimers of the Bateman domains. The two dimers are superposed over the pink monomer. Conformation A has a larger interface and is more similar to the typical interface (see in A) than conformation B. The interface of the Bateman domains in conformation B is on the opposite side of the Bateman domains than in conformation A. The structure figures were generated by using PYMOL.

domain follow the Michaelis–Menten kinetics in dependence on GMP concentration. Whereas the protozoal GMPRs bind GMP into the allosteric site in the CBS domain and show the positive cooperative kinetics in dependence on increasing GMP concentration [30,31], the Msm and Mtb GMPRs exhibit negative cooperative kinetics dependent on GMP concentration. Our X-ray structural analysis has indicated the binding of GMP only in the catalytic sites in the Msm GMPR octamer. Therefore, we hypothesise that the negative cooperative effect of GMP may rather be caused by its binding to the active site of the neighbouring subunit. The Msm GMPR $K_{0.5}$ values for GMP at pH 6.6 and 7.8 are 4.2 and 3.5 {M respectively. The corresponding $K_m$ values of biochemically characterised eukaryotic and prokaryotic GMPRs are in the range 1.5–17.5 {M [53–55,61]. Nevertheless, the determined intracellular GMP concentration in Msm cells ranges between 30 and 100 {M and is approximately 10 times higher than the corresponding $K_{0.5}$ value for this nucleotide. Therefore, the Msm GMPR reaction velocity is not likely to be limited by GMP concentration *in vivo*. The Msm GMPR $K_m$ values for the second substrate, NADPH, are 30 and 63 {M at pH 7.8 and 6.6, respectively, and they are comparable

with the corresponding $K_m$ values of characterised GMPRs [53–55,61]. The intracellular NADPH level in *Corynebacterium glutamicum*, a species similar to Msm, has been shown to be in the range 140–330 {M in dependence on nutrient availability [62]. This NADPH concentration range is still well suited for the efficient catalysis of Msm GMPR *in vivo*.

ATP and GTP, the end products of the purine biosynthesis pathway, regulate the Msm GMPR activity in a pH-dependent manner. At the optimal pH of 7.6, 1 mM GTP or ATP had only a minor effect on Msm GMPR activity. At lower pH, the positive effect of GTP and the negative effect of ATP became apparent. At pH 6.6, 1 mM GTP increased the activity by 31% and 1 mM ATP decreased it by 86%. Intracellular pH can vary in dependence on extracellular pH and the replication state of mycobacteria. Different methods have been used to detect the intracellular pH in different mycobacteria. Using radiolabelled pH probes, the intracellular pH, measured at the external pH of 5.0, was close to the value of 7 in Mtb [42]. In Msm and *Mycobacterium bovis* BCG, the intracellular pH ranged between pH 6.5 and 7 at the extracellular pH of 4–7 [40]. Under growth conditions, measurement using the pH-sensitive green fluorescent protein detected the
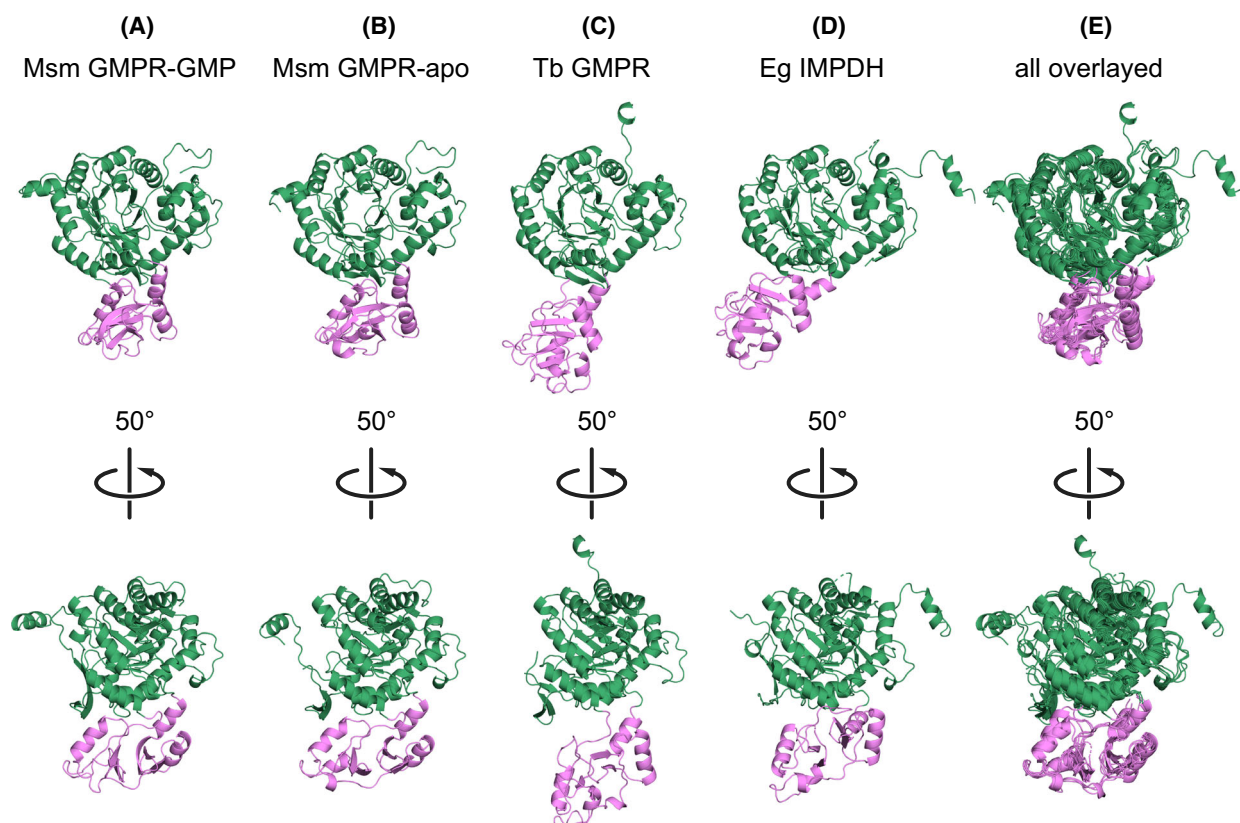
**Fig. 12.** Structure of Msm GMPR and its comparison to *Trypanosoma brucei* (Tb) GMPR and *Eremothecium gossypii* (Eg) IMPDH. Monomers of (A) Msm GMPR with bound GMP, (B) Msm GMPR apo form, (C) Tb GMPR apo form (PDB ID: 6JL8) and (D) Eg IMPDH with bound GDP and GMP (PDB ID: 4Z87). (E) Overlay of the structures where the catalytic and the CBS domains were aligned independently to compensate for differences in the quaternary structure. The catalytic domains are in green and the CBS domains in white. The structure figures were generated by using PYMOL.

intracellular pH in the range 7.3–7.6 in Mtb H37Rv [63]. However, when bacteria survive in macrophages or are cultivated *in vitro* in acidic conditions, they maintain the intracellular pH in the range 6.76–7.25 [41,64,65]. Differences in the pH of intracellular niches should also be taken into account [66]. The data available show that the intracellular pH in mycobacteria could vary between 6.5 and 7.6, which means that the GTP-positive and ATP-negative regulation of GMPR activity may function in bacteria.

Both GTP and ATP are V-type allosteric regulators, influencing the $V_{lim}$ parameter but not the $K_{0.5}$ value. In this respect, GTP can be considered as a non-essential allosteric activator and does not play a significant role. On the contrary, the negative regulation of Msm GMPR activity by ATP is more important because its higher concentration can decrease the activity even by 86%. Our metabolomic analysis showed the 4 mM intracellular ATP pool in exponentially grown Msm cells, which is similar to the ATP concentration determined in *M. bovis* [67]. However, this value is approximately two orders higher than the 50% inhibitory ATP concentration (57 μM) determined for Msm GMPR. Although the intracellular level of ATP in mycobacteria may depend on many factors, especially on hypoxia degree and nutrient availability, a decrease below 500 μM is very unlikely [67–72]. In light of these facts, the importance of GTP, which is able to reactivate the ATP-inhibited Msm GMPR, is apparent. We have shown that the full activity of the Msm GMPR inhibited by an excess of ATP (570 μM) is restored by approximately twice as high GTP concentration. The ratio of GTP and ATP concentrations can thus effectively regulate the activity of Msm GMPR, but only at slightly acidic pH. The determined concentration of GTP in Msm was 2.5 mM (Fig. 3A). Under these conditions, the Msm GMPR will be dominantly in an inhibited state.

The analysis of the oligomeric state of Msm GMPR by gel filtration revealed the effect of GMP (substrate),
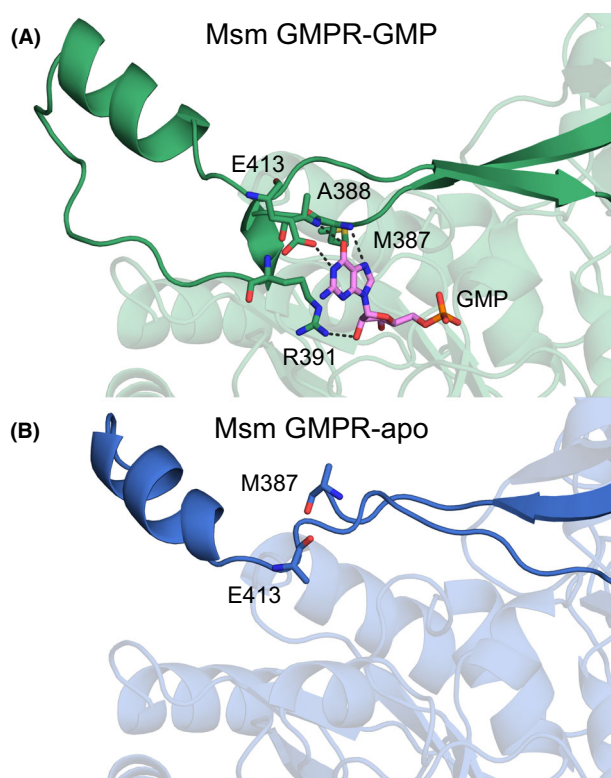
**Fig. 13.** The stabilisation of the Msm GMPR active site by GMP. (A) The binding of GMP into the active site stabilises the adjacent loop by the interaction with residues Met387, Ala388, Arg391 and Glu413. Hydrogen bonds are dashed. (B) The loop has a different conformation and is partially disordered without GMP. The structure figures were generated by using PYMOL.

IMP (product) and ATP and GTP (activity effectors) on the dissociation of octamers into tetramers at different pH values. The Msm GMPR apo form was octameric under all the conditions tested. At pH 6.6, the binding of the substrate, product or allosteric effectors led to the formation of tetramers; Msm GMPR was present in solution only as an octamer. However, at pH higher than 7, substrate or product binding did lead to the formation of a tetrameric pool, which increased with increasing pH. The binding of ATP and GTP to the Msm GMPR-GMP complex shifted the octamer/tetramer ratio back to an octameric state. A low percentage of tetramers was detected only at pH 8.2. The intracellular pH thus significantly contributes to the regulation of Msm GMPR activity and oligomeric state by the binding of allosteric effectors.

X-ray crystallography has confirmed the presence of CBS domains in Msm GMPR. Despite low sequence similarity, the individual structures of the catalytic domain and the CBS domains are very similar to other

known IMPDH and GMPR structures (Fig. 12). The quaternary structure of Msm GMPR is an octamer typical of the structures of IMPDHs and GMPRs with CBS domains. The catalytic domain forms a tetramer with the CBS domains at the perimeter, and then two tetramers form an octamer through the interaction of the CBS domains (Fig. 10).

Although the structure of Msm GMPR is similar to other structures of IMPDHs and GMPRs in many respects, it has several distinguishing features. The CBS domains in Msm GMPR are much closer to the catalytic domains and thus have a much larger interaction area. This close interaction is caused by the absence of a flexible linker, which allows independent movement of the catalytic and the CBS domains in other available IMPDH and GMPR structures (Fig. 10). Msm GMPR has crystallised in two distinct conformations (Fig. 10), which differ in the mutual orientation of the two tetramers. Since the catalytic and CBS domains in Msm GMPR cannot move independently, the changes in the mutual orientation of the tetramers have resulted in the formation of distinct dimerisation interfaces between the CBS domains (Fig. 11). The catalytic and CBS domains of the other known IMPDs and GMPRs can move independently, as a consequence of which the different orientation of the tetramers does not influence the CBS dimer and its conformation (Fig. 11). In several IMPDHs and GMPRs, the changes in the mutual orientation of the tetramers are induced by ligand binding. However, we have excluded that the conformational changes in the crystal structures of Msm GMPR could have been caused by GMP binding, pH or some other known crystallisation conditions. We suggest that the mutual orientation of the two tetramers in the octamer is a result of the crystal packing because it correlates with the space group of the crystals. Msm GMPR with or without GMP has crystallised in four different space groups regardless of the crystallisation conditions. Therefore, the space group of the crystal has probably been determined by some local condition, such as the amount of the precipitate in the area of crystal nucleation. This also implies that neither of the CBS-domain dimerisation interfaces is strong enough to overcome crystal packing forces during crystallisation. A much more extensive set of structures in different space groups would probably be necessary to show whether the GMP, or any other ligand, has at least some effect on the mutual orientation of the tetramers. Even if the structures cannot be properly refined because of the low quality of the crystals, it is possible to show in which conformation the protein is. In our opinion, it is the close and fixed position of the
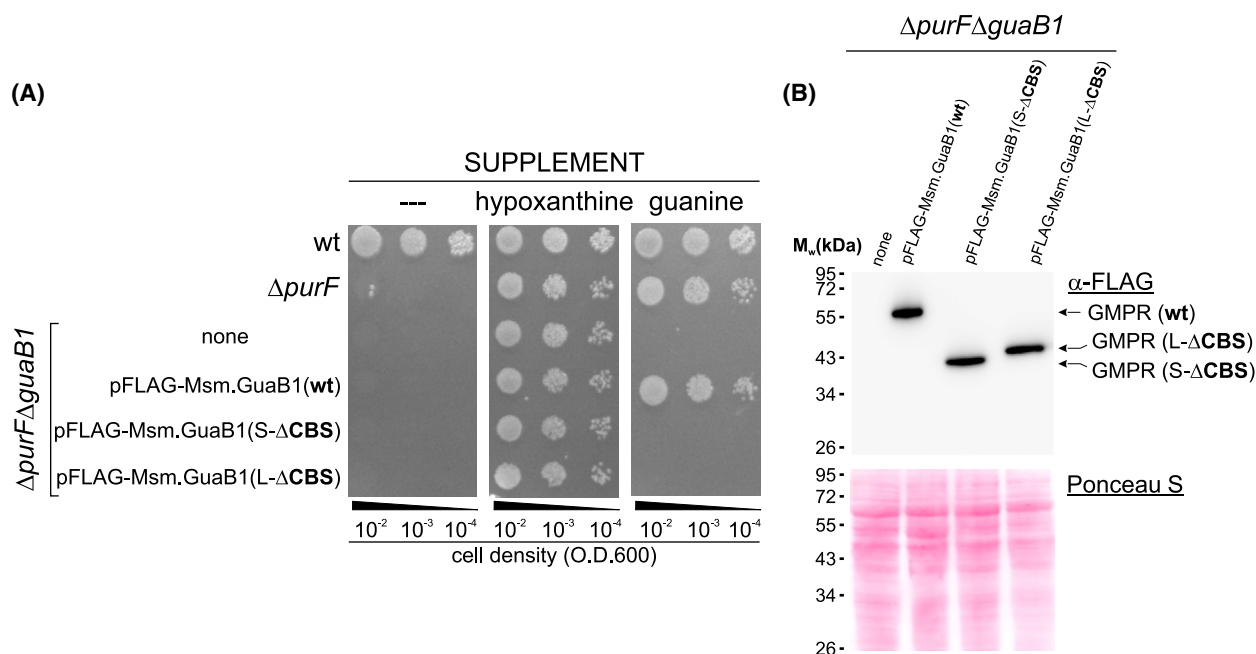
**Fig. 14.** The importance of the CBS domain for Msm GMPR. (A) The *ΔguaB1ΔpurF* Msm strain was transformed with pFLAG plasmid carrying genes for wt and ΔCBS GMPR variants (S and L). *ΔguaB1ΔpurF* parental strain and its transformants, *ΔpurF* and wt strains, were analysed for growth in the absence and presence of 100 μM hypoxanthine or guanine on the 7H10/ADC medium. (B) The immunoblot analysis of the crude lysates of the *ΔguaB1ΔpurF* parental strain and its transformants using α-FLAG antibody.

catalytic and the CBS domains that is responsible for at least some of the unique properties of Msm GMPR.

We found bound GMP only in the active site of Msm GMPR, and the orientation of GMP in the active site is virtually identical to that in other structures of IMPDHs and GPMRs (Fig. 13). The binding of GMP stabilises the loop covering the active site by the interaction with residues Met387, Ala388, Arg391 and Glu413. The stabilisation of this loop by purine nucleotide monophosphate binding is often observed in the structures of IMPDHs and GMPRs [13,24,25,33] and is considered important for the activity of the proteins [19].

The stabilisation of the loop may explain the influence of GMP on the oligomerisation of Msm GMPR and its other properties. We have shown that the binding of GMP has caused the dissociation of Msm

GMPR octamers (Fig. 8). Since the loop can interact with the CBS domains from the neighbouring and the opposing monomers, it is possible that conformational changes in the loop can cause changes in the mutual orientation of the tetramers and thus influence their dissociation. It is also possible that the stabilisation of the loop in one monomer affects the conformation of the loop in other monomers through interactions with the CBS domains. This can explain the cooperative kinetics dependent on the GMP concentration. Furthermore, the unique position of the CBS domains in Msm GMPR can be one of the reasons for the negatively cooperative kinetics, occurring only in Mtb and Msm GMPRs.

Based on the two structures presented, we can speculate about the ATP and GTP effect on the activity and oligomerisation of Msm GMPR. It is possible that

**Fig. 15.** (A) A phylogenetic tree constructed from GuaB1 homologues found throughout the Actinobacteria phylum. For clarity, the tree shows only a fraction of the organisms from the 12 orders. Orders are visually distinguished by colour; the family is indicated by the abbreviation in front of the name of the organism. Homologues have been chosen to capture the diversity of the homologous sequence within the entire phylum and to show interrelationships. Blue dots represent the bootstrap value of replicate trees above 0.5. (B) The conservation of GuaB1 across the Actinobacteria phylum. The height of the letters indicates the level of amino acid conservation; the colour of individual letters follows the CLUSTALX convention. The consensus of the sequences aligned by the MUSCLE algorithm used for building a phylogenetic tree has the same domain composition as the *Mycobacterium smegmatis* GuaB1 protein sequence. The pink and yellow shadings indicate the catalytic and CBS domains respectively.

**(A)**

Tree scale: 0.1 ⊢———⊣



**(B)**
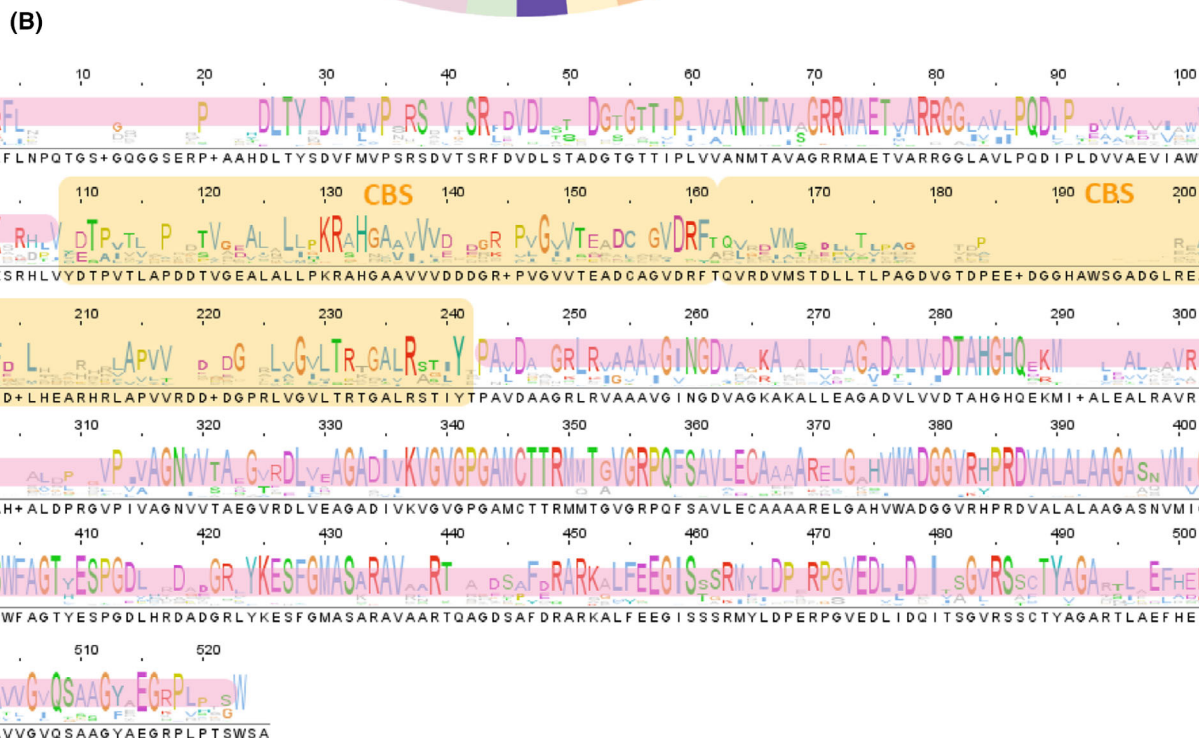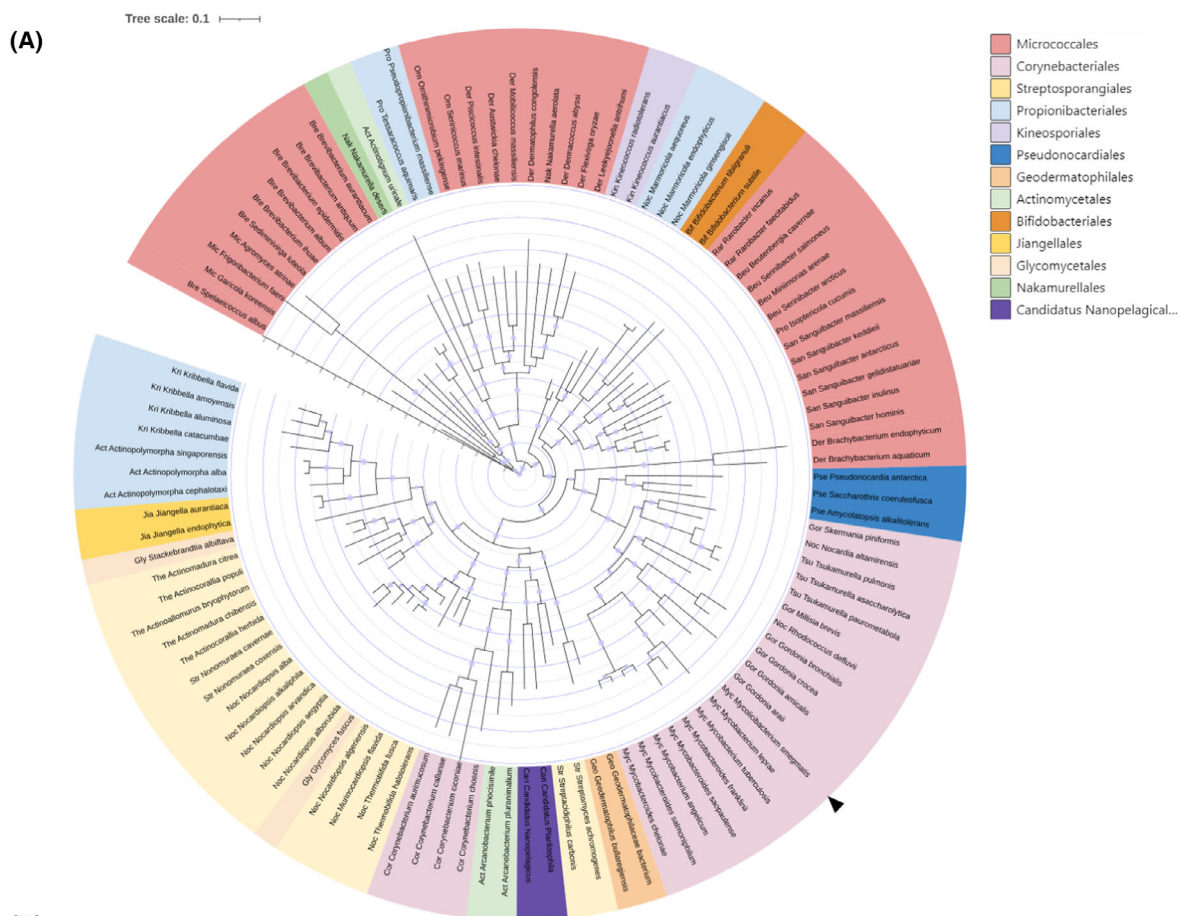
in solution, where the conformation is not restricted by crystal packing, the mutual orientation of the two tetramers can be influenced by ligand binding to the CBS domains, by pH or other factors. GTP and ATP could preferentially stabilise different conformations of the CBS dimers and thus influence the conformation of the loop covering the active site and subsequently the activity. However, future studies are necessary to elucidate the precise mechanism.

Taken together, our data show that the Msm *guaB1* gene encodes a functional guanosine 5′-monophosphate reductase with a CBS domain and that its orthologues are spread across the Actinobacteria phylum. Its activity is negatively regulated by ATP and positively by GTP based on pH. Although the Msm GMPR is not essential for Msm viability, it may contribute to the regulation of the purine nucleotide pool by recycling GMP to IMP.

## Materials and methods

### DNA constructs

For all cloning procedures, we used Q5 polymerase (NEB, Ipswich, MA, USA) for PCR DNA amplification and *E. coli* DH5α for plasmid amplification. T4 DNA ligase and restriction endonucleases were purchased from NEB. The ligation of DNA fragments was performed using In Fusion™ cloning (Takara, Shiga, Japan). The final constructs were verified by Sanger sequencing (EUROFINS, Hamburg, Germany). Primer sequences (Generi Biotech, Hradec Králové, Czech Republic) are listed in Table 3.

Specific Msm *guaB1* and *guaB2* deletion cassettes (designated as pYS2-Δ*guB1* or pYS2-Δ*guaB2*) were based on the pYS2 plasmid, which contains the *Spe*I/*Swa*I-*loxP*-*gfp*-*hyg*ʳ-*loxP*-*Pac*I/*Nsi*I selection locus [73]. The regions upstream of *guaB1* (703 bp) and *guaB2* (889 bp) were amplified by PCR using Msm chromosomal DNA as a template with the primer pairs 1/2 and 5/6, respectively, and ligated into pYS2 via *Spe*I/*Swa*I sites. Subsequently, 829-bp *guaB1* and 747-bp *guaB2* downstream regions were amplified by PCR with the primer pairs 3/4 and 7/8, respectively, and ligated into the corresponding pYS2 intermediate via *Pac*I/*Nsi*I sites. The construction of the deletion plasmid pYS2-Δ*purF* has been described previously [43].

Msm and Mtb GMPR complementation expression plasmids were constructed on the basis of the *attB*-site integrable pFLAG vector containing a constitutive *tet* promoter in the absence of a Tet repressor [74]. The pFLAG-Msm.GuaB1 and pFLAG-Mtb.GuaB1 plasmids were constructed as follows: *Msm.guaB1* and *Mtb.guaB1* were amplified from genomic DNA by PCR using the primer pairs 9/10 and 11/12, respectively, and the fragments were inserted

**Table 3.** List of primers used in this study.

| Primer | Sequence (5′–3′) | Orientation[a] | Restriction site |
|---|---|---|---|
| 1[b] | aaa<u>ACTAGT</u>tggtcgatgtgatcgtcgacgag | F | *Spe*I |
| 2[b] | ttt<u>ATTTAAAT</u>ggagtcgaatctactcaggcctcga | R | *Swa*I |
| 3[b] | aaa<u>TTAATTAA</u>aactgcacgagaaggtggtgctc | F | *Pac*I |
| 4[b] | ttt<u>ATGCAT</u>acctgagcgtcggtggcaacgt | R | *Nsi*I |
| 5[b] | aaa<u>ACTAGT</u>aagaagagcccgcagagccg | F | *Spe*I |
| 6[b] | ttt<u>ATTTAAAT</u>aacgctgctttcagcgatcgacat | R | *Swa*I |
| 7[b] | aaa<u>TTAATTAA</u>acaggggggacccttcagtcatg | F | *Pac*I |
| 8[b] | ttt<u>ATGCAT</u>gtggccatcgggacgctgat | R | *Nsi*I |
| 9 | GATATACATATGAGTGTGAGGTTTCTTGACGGACACACGCCC | F | – |
| 10 | GTCTTTGTAGTCTGCCCAGCCGGCGGGTAGCGG | R | – |
| 11 | GATATACATATGAGTatgagatttctagacgggcacc | F | – |
| 12 | GTCTTTGTAGTCTGCccagccggcggg | R | – |
| 13 | GGAGGTCTGCGCATCGCTGCGGCCGTC | F | |
| 14 | ATGCGCAGACCTCCGCTCTTGACGAAGTCGACGGTCTCGCTGAC | R | |
| 15 | TCGGGAGGTACGCGCACGGGGGCGATCCGGGCGGG | F | |
| 16 | GCGCGTACCTCCCGACACCAGATCGCGGCTCTTGACGAAGTCGACGGT | R | |
| 17 | ACCGCTGCTGCGAAAGAGGATCTCGAGCACCACCATCACCA | F | |
| 18 | CATGGTATATCTCCTTTGATTGTAAATAAAATGTAATTTA | R | |
| 19 | CAATCAAAGGAGATATACCATGGTGAGGTTTCTTGACGGACACACGCCC | F | |
| 20 | TTTCGCAGCAGCGGTCCAGCCGGCGGGTAGCGGATG | R | |
| 21 | ATGCTTAATTAACAGCTGATTTatgagatttctagacgggcacccacccgggta | F | |
| 22 | CCGGGGGATCCATTTTTAGTGATGGTGATGGTGATGG TGGTGCTCGAGATCCTCTTTCGCAGCAGCGGTccagccggcgggcagcggatggcc | R | |

<sup>a</sup>F, forward direction; R, forward direction.

<sup>b</sup>Corresponding restriction sites are in a capital letters

into *Sap*I-linearised pFLAG by the in-fusion approach. The pFLAG-Msm.GuaB1(S-ΔCBS) encoding GuaB1 lacking the region R92-R214, with it being replaced by the GG motif, was constructed as follows: pFLAG-Msm.GuaB1 was PCR linearised by the primer pair 13/14 and circularised by the in-fusion approach. The pFLAG-Msm.GuaB1 (L-ΔCBS) encoding GuaB1 lacking the region V96-L194, with it being replaced by the SGG motif, was constructed as follows: pFLAG-Msm.GuaB1 was PCR linearised by the primer pair 15/16 and circularised by the in-fusion approach. The plasmid encoding of C-terminally His-tagged Mtb GMPR for expression in Msm was based on the pSE200 vector [44], derived from the pSE100 plasmid containing a constitutive *Pmyc1tetO*-promoter in the absence of a Tet repressor [75]. *Mtb.guaB1His* was amplified from genomic DNA by PCR using the primer pair 21/22 and inserted into *Swa*I-linearised pSE200 by the in-fusion approach. *E. coli* expression pTriex-Msm.GuaB1 plasmid was constructed as follows: the *Msm guaB1* gene was amplified by PCR by the primer pair 19/20 and inserted into the PCR-linearised pTriex-4 vector (Novagen, Madison, WI, USA) with the primers 17/18 by the in-fusion approach.

## The cultivation of *M. smegmatis*

The *M. smegmatis* mc$^2$ 155 strain and its mutants were propagated in liquid 7H9 medium (Sigma-Aldrich, Burlington, MA, USA) with 10% ADC supplement (5% BSA, 0.85% NaCl and 2% dextrose) and 0.05% tyloxapol or 7H10-ADC agar medium (Sigma-Aldrich) at 37 °C. In both cases, the carbon source was enriched with 0.5% (vol/vol) glycerol. Hygromycin and kanamycin were added at final concentrations of 150 and 25 μg·mL$^{-1}$ respectively. Purine supplements (adenine, guanine and hypoxanthine) were prepared as 75 mM stocks in DMSO and were added to a final concentration of 200 μM when required.

## Gene deletion

Gene disruption using a pYS2 deletion plasmid was performed as previously described [73]. Briefly, the *Spe*I/*Nsi*I-linearised pYS2-Δ*guaB1* or pYS2-Δ*guaB2* deletion cassette was introduced into electrocompetent *M. smegmatis* cells with 0.2% acetamide-driven expressed Chec9 DNA by electroporation. Msm recombinants were obtained by selection on the 7H10/ADC medium containing hygromycin at 42 °C for 3 days. In the case of the *guaB2* gene, the medium was supplemented with 200 μM guanine. To remove the Hyg$^r$ cassette, gene disruptants were transformed with the pML2714 vector, which constitutively expresses Cre recombinase. Deletions were screened by PCR using Q5 polymerase and primer pairs that anneal at the boundaries of the deleted regions, and amplicons were sequenced. In the Δ*guaB2* strain, the second deletion of the *purF* gene was not cleared from the Hyg$^r$ cassette.

## Metabolite analysis

The 7H9/ADC medium (100 mL in a 500-mL Erlenmeyer cultivation flask) was inoculated with a fresh culture of Msm at the stationary phase (O.D.$_{600}$ = 10) to an initial O.D.$_{600}$ of $10^{-3}$. The cell suspension was grown to an O.D.$_{600}$ of 0.5 at 37 °C and 200 r.p.m. (15–18 h). Subsequently, 3 mL of the cell suspension was quickly vacuum filtered through a 0.45 μm/25 mm cellulose acetate filter. The membrane with the collected bacteria was immediately transferred into 1 mL of ice-cold 1 M acetic acid in a 1.5-mL microtube and quickly frozen in liquid nitrogen. The samples were slowly thawed on ice and then incubated on the ice for 30 min with short vortexing at 5-min intervals. The crude bacterial lysate was separated from the filter by centrifugation (4000 *g*, 30 s) through a pinhole at the bottom of the 1.5-mL microtube inserted into a 2-mL collection tube. The lysate was flash frozen in liquid nitrogen and lyophilised. The material was then resuspended in 200 μL of ice-cold deionised water and incubated on ice for 30 min. Insoluble material was removed by centrifugation at 22 000 *g* for 20 min at 4 °C. A clear aqueous bacterial extract was collected and stored at −80 °C for subsequent analysis. The analysis of Msm extracts was performed on cZIC-HILIC columns (150 × 2.1 mm) with a flow rate of 0.3 mL·min$^{-1}$. Mobile phase A was 10 mM ammonium acetate, pH 5, adjusted with acetic acid. Mobile phase B was 10 mM ammonium acetate, pH 5, and 90% acetonitrile. MS quantification was performed by negative electrospray ionisation with the following parameters: capillary voltage = 2 kV, cone voltage = 20 V, source temperature = 120 °C, desolvation temperature = 400 °C, desolvation gas flow = 400 L·h$^{-1}$ and cone gas flow = 30 L·h$^{-1}$.

The intracellular concentrations of metabolites were calculated from Eqn (1), where [metabolite]$_{ex}$ is the concentration of the metabolite in the extract in μM, $V_{ex}$ is the volume of the extract (μL), OD is the optical density of the cell suspension and $V_C$ is the volume of the filtered cell suspension (mL). NC ($2.3 \times 10^7$ mL$^{-1}$) is the number of cells in 1 mL of cell suspension at O.D.$_{600}$ = 0.1; it has been determined by a colony forming unit assay. $V_{cell}$ ($5.2 \times 10^{-6}$ μL) is the volume of a rod-shaped mycobacterial cell of the average dimensions 5.5 × 1.1 μm.

$$[\text{metabolite}]_{in} = [\text{metabolite}]_{ex} \times \frac{V_{ex}}{\text{OD} \times V_C \times \text{NC} \times V_{cell}}.$$
(1)

## Growth curve

Three hundred and thirty microlitre of the 7H9/ADC medium in a honeycomb 100-well cultivation Bioscreen C plate (Growth Curves Ltd., Helsinki, Finland) was inoculated by 20 μL of Msm exponentially growing cells to the initial O.D.$_{600}$ of 0.005. Bacterial growth was monitored at 37 °C and 400 r.p.m. shaking speed by measuring the

O.D.$_{600}$ in 15-min intervals. The real O.D.$_{600}$ for the 1 cm optical path value was calculated by the calibration curve using the Msm culture standards of the known O.D.$_{600}$ accessed on a BioPhotometer plus spectrophotometer in a 1-cm cuvette (Eppendorf Ltd., Hamburg, Germany).

## Nutrient starvation

Ten millilitre of the exponentially growing cells (O.D.$_{600}$ in range 0.2–0.5) were centrifuged at 2000 *g* for 5 min at room temperature. Five millilitre of sterile deionised water was used for four washing steps and the cell pellet was finally resuspended in 1 mL of water. Bacterial suspension was used for the inoculation of 5 mL starvation buffer (10 mM NaH$_2$PO$_4$, 4 mM KCl, 120 mM NaCl and 0.1% tyloxapol; the pH was adjusted by NaOH to pH 5.5 or 6.9) in 12-mL screw-cap glass tubes (Carl Roth GmbH+Co., Karlsruhe, Germany) with a 4-mm magnetic Teflon stirrer to the final c.f.u. ~ 10$^6$ c.f.u.mL$^{-1}$. Bacterial suspensions were cultivated at 37 °C under mild stirring (100 r.p.m.), and viable cells at individual time points of the starvation were determined by plating serially diluted culture aliquots on the 7H10/ADC medium.

## Nucleotide ligands

The sodium salts of GMP, IMP, XMP and NADPH were purchased from Santa Cruz (Dallas, TX, USA), the sodium salts of ATP and GTP from Sigma. Except for NADPH, the compounds were dissolved in deionised water to the final concentrations of 50–100 mM. The pH of the ATP and GTP stocks was immediately adjusted to pH 7.0 with 1 M NaOH. The exact concentrations of the stocks were determined spectrophotometrically at the absorption maxima using the following absorption coefficients: $\varepsilon^{260 \, nm}$ (ATP) of 15.4 mM$^{-1}$·cm$^{-1}$, $\varepsilon^{253 \, nm}$ (GTP, GMP) of 13.7 mM$^{-1}$·cm$^{-1}$, $\varepsilon^{263 \, nm}$ (XMP) of 8.6 mM$^{-1}$·cm$^{-1}$ and $\varepsilon^{249 \, nm}$ (IMP) of 12.1 mM$^{-1}$·cm$^{-1}$. The stocks were aliquoted and stored at −70 °C. NADPH was dissolved in deionised water directly before the measurements to create a 20 mM solution. The exact concentration was determined spectrophotometrically at 340 nm using the extinction coefficient $\varepsilon^{340 \, nm}$ (NADPH) of 6.3 mM$^{-1}$·cm$^{-1}$.

## Protein expression and purification

Recombinant Msm GMPR with uncleavable C-terminal and N-terminal histidine tags, respectively, was produced in *E. coli* BL21(DE3) RIL cells. The ZYM-505 medium [76] containing ampicillin (50 μg·mL$^{-1}$) was inoculated with an overnight culture of cells carrying the appropriate expression plasmid to an initial O.D.$_{600}$ of 0.1. The resulting culture was cultivated at 37 °C to an O.D.$_{600}$ of 2.0–3.0. The temperature was then lowered to 18 °C and expression was induced by 0.4 mM IPTG. The cells were harvested 16 h after induction

at 8000 *g* for 10 min. The cell pellet was resuspended in lysis buffer (200 mM potassium phosphate, pH 8.0, 2 M potassium chloride, 2.5 mM TCEP, 10 mM imidazole, 0.5% Triton X-100, 1 mM PMSF and 0.1 mg·mL$^{-1}$ lysozyme) and stirred at 4 °C for 60 min. The lysate was sonicated, and the insoluble fraction was removed by centrifugation at 35 000 *g* for 30 min. The supernatant was loaded onto an immobilised metal affinity chromatography column (HiTrap IMAC HP 5 mL) charged with Ni$^{2+}$ and equilibrated with buffer A (200 mM potassium phosphate, pH 8.0, 2 M potassium chloride and 2.5 mM TCEP) containing 10 mM imidazole. The column was washed with buffer A containing 82.5 mM imidazole, and the His-tagged proteins were eluted with buffer A containing 300 mM imidazole. Msm GMPR and Msm CBS were next purified by size-exclusion chromatography using HiLoad 26/60 Superdex 200 pg and HiLoad 26/60 Superdex 75 pg columns in buffer A respectively. The purified proteins were transferred into storage buffer (50 mM Tris, pH 8.0, 2.5 mM TCEP) by desalting (HiPrep 26/10 Desalting) and concentrated to 25 mg·mL$^{-1}$ by centrifugal ultrafiltration. Finally, the proteins were aliquoted and stored at −70 °C. All purification procedures were performed on ice or at 4 °C. All FPLC equipment was manufactured by GE Healthcare Life Sciences (Chicago, IL, USA). The purity of the target proteins was analysed by SDS/PAGE, and the identity of the proteins was confirmed by mass spectrometry. The concentration and identity of copurified nucleotide 5′-monophosphates were determined by HPLC.

Recombinant Mtb GMPR with an uncleavable C-terminal His tag was produced in Msm with a deleted *guaB1* gene (*ΔguaB1*) under the control of the constitutive Psmyc promoter. The Msm *ΔguaB1* strain transformed with plasmid pSE200-Mtb.GuaB1.His was cultivated in the LB medium containing 0.1% (w/v) tyloxapol and 0.5% (w/v) glycerol until the O.D.$_{600}$ reached 10. The cell pellet from 5 L of media was resuspended in 200 mL of lysis buffer and disintegrated by three passes on a French press at a pressure of 1500 psi. The crude lysate was centrifuged at 50 000 *g* for 40 min. The supernatant was loaded onto an immobilised metal affinity chromatography column (HiTrap IMAC HP 5 mL) charged with Ni$^{2+}$ and equilibrated with buffer A containing 50 mM imidazole. The column was washed with buffer A containing 100 mM imidazole, and the His-tagged Mtb GMPR was eluted with buffer A containing 300 mM imidazole. Purified Mtb GMPR was desalted into storage buffer using a PD10 column (GE Healthcare), concentrated to 2 mg·mL$^{-1}$ by centrifugal ultrafiltration, aliquoted and stored at −70 °C. All purification steps were carried out at 4 °C.

## Enzyme kinetics

All enzymatic reactions were carried out in MPH buffer composed of 30 mM MES (2-(*N*-morpholino) ethanesulfonic acid), 30 mM HEPES (2-[4-(2-hydroxyethyl) piperazin-1-yl]ethanesulfonic acid),

20 mM PIPES (2-[4-(2-sulfoethyl)piperazin-1-yl]ethanesulfonic acid), 100 mM KCl and 2 mM DTT and adjusted to the appropriate pH with 10 M NaOH. Msm GMPR was used in the concentration range 20–100 nM; the actual concentrations are stated for individual experiments. Msm GMPR did not show any deviations in specific activity in this concentration range. The data were processed with GRAPHPAD PRISM 7 software (GraphPad Software Inc., San Diego, CA, USA).

The initial reaction velocity of the GMPR reaction was determined from the decrease in NADPH absorbance at 340 nm during the reaction. The absorbance was measured in 20-s intervals for 30–60 min in a 1-cm quartz cuvette at $25 \pm 0.1$ °C using a Specord 200 PLUS spectrophotometer (Analytik Jena GmbH, Jena, Germany). The slope of the decrease was calculated from the linear part of the steady state of the absorbance curve by least-squares linear regression. The initial reaction velocity ($s^{-1}$) was then calculated from Eqn (2):

$$v_0 = \frac{|\text{slope}_E - \text{slope}_{\text{blank}}|}{[E] \cdot \epsilon}, \qquad (2)$$

where $\text{slope}_E$ and $\text{slope}_{\text{blank}}$ are the slopes of the absorbance decrease at ($A \cdot s^{-1}$) for a reaction mixture containing Msm GMPR, NADPH and GMP or for a blank mixture containing only Msm GMPR and a corresponding concentration of NADPH under the same conditions (pH, ionic strength, etc.) respectively. $[E]$ is the molar concentration of Msm GMPR in nM and $\epsilon$ is the absorption coefficient of NADPH at 340 nm in $nM^{-1} \cdot cm^{-1}$ units ($6.22 \times 10^{-6}$).

The kinetic parameters of Msm GMPR were determined at pH 7.6 and 6.6. A reaction mixture containing NADPH and GMP in MPH buffer was equilibrated to 25 °C, and the reaction was started by the addition of 20 nM Msm GMPR. The parameters of the reaction at a fixed GMP concentration (100 μM) were calculated from the initial reaction velocities for the concentrations of NADPH in the range 10–200 μM using Eqn (3).

$$v_0 = \frac{V_{\text{lim}} \cdot [S]}{K_m + [S]} \qquad (3)$$

The parameters of the reaction at a fixed NADPH concentration (200 μM) were calculated from the initial reaction velocities for the concentrations of GMP in the range 1–500 μM using Eqn (4).

$$v_0 = \frac{V_{\text{lim}} \cdot [S]^n}{K_{0.5}^n + [S]^n} \qquad (4)$$

The inhibition constants for XMP and IMP at a fixed NADPH concentration (200 μM) were calculated from the initial reaction velocities for the concentrations of GMP in the range 5–100 μM using Eqn (5). The parameters $K_i$, $V_{\text{lim}}$ and $K_m$ were shared for all IMP (0–200 μM) and XMP (0–5 μM) concentrations.

$$v_0 = \frac{V_{\text{lim}} \cdot [S]}{K_m \cdot \left(1 + \frac{[I]}{K_i}\right) + [S]} \qquad (5)$$

The effect of pH on the activity of Msm GMPR in the presence of ATP or GTP was measured as follows: 250 μL of 200 nM Msm GMPR in MPH buffer containing 2 mM MgCl$_2$ at the given pH were preincubated without a ligand or with 1 mM GTP or ATP at 25 °C for 30 min. The reaction was started by the addition of 250 μL of a preheated twice concentrated substrate mix containing 200 μM GMP and 400 μM NADPH in the same buffer (including 1 mM GTP or ATP as appropriate). The activity at the given pH was expressed as the relative activity calculated from Eqn (6):

$$\text{relative activity}_{\text{pH}} = \frac{(v_0)_{\text{pH}}^{\text{NTP}}}{(v_0)_{\text{pH}}^{\text{ctrl}}} \qquad (6)$$

where $(v_0)_{\text{pH}}^{\text{NTP}}$ and $(v_0)_{\text{pH}}^{\text{ctrl}}$ are the initial velocities of the reaction at the given pH in the presence or absence of the ligand respectively. The relative activities were plotted against pH and fitted with a linear (GTP) or Hill equation (ATP).

The effect of ATP concentration (1–125 μM) on Msm GMPR activity at pH 6.6 was measured as follows: 250 μL of 200 nM Msm GMPR in MPH buffer containing 2 mM MgCl$_2$ was preincubated with ATP at 25 °C for 30 min. The reaction was started by the addition of 250 μL of a preheated twice-concentrated substrate mix (200 μM GMP and 400 μM NADPH) with the same ATP concentration. The activity at the given ATP concentration was expressed as the relative activity calculated from Eqn (7):

$$\text{relative activity}_{[\text{ATP}]} = \frac{(v_0)_{[\text{ATP}]}}{(v_0)_{\text{ctrl}}} \qquad (7)$$

where $(v_0)_{[\text{ATP}]}$ and $(v_0)_{\text{ctrl}}$ are the initial velocities of a reaction containing ATP at a given concentration and a control reaction without ATP respectively. The relative activity was plotted against ATP concentration and fitted with the Hill equation.

The ability of GTP to restore partially or fully ATP-inhibited Msm GMPR at pH 6.6 was measured as follows: 250 μL of 200 nM Msm GMPR in MPH buffer containing 2 mM MgCl$_2$ was preincubated with 57 μM (partial inhibition) or 570 μM ATP (complete inhibition) at 25 °C for 30 min. The reaction was started by the addition of 250 μL of a preheated twice-concentrated substrate mix (200 μM GMP and 400 μM NADPH) with ATP (57 or 570 μM) and GTP (twice final concentration). The activity at the given GTP concentration was expressed as the relative activity calculated from Eqn (8):

$$\text{relative activity}_{[\text{GTP}]}^{[\text{ATP}]} = \frac{(v_0)_{[\text{GTP}]}^{[\text{ATP}]}}{(v_0)_{\text{ctrl}}} \qquad (8)$$

where $(v_0)_{[GTP]}^{[ATP]}$ is the initial velocity of a reaction containing ATP (57 or 570 μM) and GTP (0–1 mM), and $(v_0)_{ctrl}$ is the initial velocity of a control reaction without ATP or GTP. The relative activity was plotted against GTP concentration and fitted with the Hill equation.

## Chromatographic analysis of the GMPR reaction mixture

Mixtures containing 75 μM NADPH and 100 μM GMP with or without 50 nM purified GMPR in MPH buffer (pH 7.6) in a total volume of 500 μL were incubated at 25 °C for 30 min. To remove the protein, 200 μL of the mixtures was passed through a minispin Amicon 3-kDa cut-off centricon (Millipore, Burlington, MA, USA). The filtrate was analysed by UPLC using an ACQUITY HSS T3 column (Waters, Milford, MA, USA) equilibrated with a mobile phase composed of 50 mM potassium phosphate (pH 3.1) and 3 mM tetrabutylammonium bisulfite at a flow rate of 0.4 mL·min$^{-1}$. After the sample was loaded, a linear gradient of 5–30% acetonitrile per 10 min was applied. The elution was monitored spectrophotometrically at 200–360 nm using a diode array detector. The compounds were assigned to individual elution peaks based on 50-μM calibration standards for NADPH, NADP$^+$, GMP and IMP.

## Analytical size-exclusion chromatography

The influence of selected ligands on the oligomeric state of Msm GMPR was analysed by size-exclusion chromatography (Superdex 200 Increase 10/300 GL, 1 mL·min$^{-1}$, 25 °C). Frozen aliquots of the concentrated protein were diluted with running buffer (45 mM MES, 30 mM PIPES, 45 mM HEPES, 100 mM KCl, 0.5 mM TCEP and 2 mM MgCl$_2$) containing appropriate ligands. The final concentration of the loaded protein was 2.5 mg·mL$^{-1}$ and the final volume was 10 μL. Protein elution was monitored by UV absorbance at 280 or 295 nm with respect to the absorption properties of the ligand. The chromatographic data were processed with FITYK software [77]. The data were normalised and then fitted with an exponentially modified Gaussian function. The oligomeric state of the protein was expressed as the percentage of protein-forming tetramers.

## Protein crystallisation

The initial conditions for MsmGMPR crystallisation were screened with MORPHEUS (Molecular Dimensions, Altamonte Springs, FL, USA) and JSCG Core I Suite (QIAGEN, Germantown, MD, USA) protein crystallisation screening kits.

Crystals were grown in a mixture of 0.3 μL protein solution and 0.3 μL reservoir solution in sitting drops at 19 °C in 96-well plates. The crystallisation trials were set up with a Mosquito Crystallisation Workstation (SPT Labtech, Melbourn, UK). The initial conditions were further optimised by changing the protein concentration, buffer pH and precipitant concentration. The final crystals were grown in drops containing 22 mg·mL$^{-1}$ MsmGMPR, 0.03 M MgCl$_2$, 0.03 M CaCl$_2$, 20% ethylene glycol, 10% PEG 8000 and 0.1 M Tris/bicine, pH 8.3. The harvested crystals were flash frozen in liquid nitrogen.

## Data collection and structure determination

The data were collected at the MX14.2 beamline at BESSY, Berlin, Germany [78], and processed using XDS [79] with XDSAPP GUI [80]. The initial structure was obtained by molecular replacement using the structure of the catalytic domain of the inosine monophosphate dehydrogenase from *S. pyogenes* (PDB ID 1ZFJ) as a model [81]. The initial structure was then improved by iterative manual rebuilding in COOT [82] and automatic refinement in PHENIX.REFINE [83,84]. The Bateman domains were built manually in the process. The final refined structure was validated with MOLPROBITY [85]. Data collection and refinement statistics are summarised in Table 2. The structure figures were generated by using the PYMOL Molecular Graphics System, Version 2.3.0 (Schrödinger, L.L.C., New York, NY, USA)

## GuaB1 tree reconstruction and consensus sequence

Sequences for phylogenetic analysis were retrieved from the NCBI non-redundant protein sequence (nr) database using the similarity search program BLASTP (similarity matrix BLOSSUM 62) [86]. The domain composition of the sequences was obtained from the Conserved Domain Database (CDD) [87] and served to confirm the identity of GuaB1. The sequences were filtered, redundant sequences were removed and the number of the sequences used to construct the phylogenetic tree was reduced by random selection to maintain the diversity representing the different orders of Actinobacteria. The analysis was performed on the PHYLOGENY.FR platform [88]. Sequences were aligned with MUSCLE (v3.8.31) [89]. Ambiguous regions were removed with GBLOCKS (v0.91b) [90] with the following settings: no gaps were allowed in the final alignment; the minimum number of sequences for a flank position was 85% and contiguous non-conserved positions larger than 8 were removed. The phylogenetic tree was reconstructed using the maximum-likelihood method [91]. The gamma parameter was estimated from the data (gamma = 0.733). Internal branch reliability was assessed by the aLRT test (SH-Like). The phylogeny tree was visualised with the ITOL platform [92]. The domain composition of the consensus sequence was explored using INTERPROSCAN [93]. The consensus logo and visualisation were created in JALVIEW (v2.11.1.4) [94].

## Acknowledgements

## Conflict of interest

The authors declare no conflict of interest.

## Author contributions

ZK, MDo and IP contributed to conceptualisation; ZK, MDo, KC, MK, MDe, EZ and DR contributed to investigation; ZK, MDo, KC, MK and EZ contributed to formal analysis; ZK and MDo contributed to writing—original draft:; IP contributed to writing—review and editing; IP contributed to funding acquisition.

## Peer review

The peer review history for this article is available at https://publons.com/publon/10.1111/febs.16448.

## Data availability statement

The structural data that support these findings are openly available in the wwPDB at https://doi.org/10.2210/pdb7OY9/pdb and https://doi.org/10.2210/pdb7R50/pdb.

## References

1 el Kouni MH. Potential chemotherapeutic targets in the purine metabolism of parasites. *Pharmacol Ther*. 2003;**99**:283–309.

2 Malathi VG, Ramakrishnan T. Biosynthesis of nucleic acid purines in *Mycobacterium tuberculosis* H37rv. *Biochem J*. 1966;**98**:594–5970.

3 Bandekar AC, Subedi S, Ioerger TR, Sassetti CM. Cell cycle-associated expression patterns predict gene function in mycobacteria. *Curr Biol*. 2020;**30**:3961–71.e6.

4 Keer J, Smeulders MJ, Williams HD. A *purF* mutant of *Mycobacterium smegmatis* has impaired survival during oxygen-starved stationary phase. *Microbiology (Reading)*. 2001;**147**:473–81.

5 Wheeler PR. Biosynthesis and scavenging of purines by pathogenic mycobacteria including *Mycobacterium leprae*. *J Gen Microbiol*. 1987;**133**:2999–3011.

6 Ducati RG, Breda A, Basso LA, Santos DS. Purine salvage pathway in *Mycobacterium tuberculosis*. *Curr Med Chem*. 2011;**18**:1258–75.

7 Cox JA, Mugumbate G, Del Peral LV, Jankute M, Abrahams KA, Jervis P, et al. Novel inhibitors of *Mycobacterium tuberculosis* GuaB2 identified by a target based high-throughput phenotypic screen. *Sci Rep*. 2016;**6**:38986.

8 Gollapalli DR, MacPherson IS, Liechti G, Gorla SK, Goldberg JB, Hedstrom L. Structural determinants of inhibitor selectivity in prokaryotic IMP dehydrogenases. *Chem Biol*. 2010;**17**:1084–91.

9 Hedstrom L, Liechti G, Goldberg JB, Gollapalli DR. The antibiotic potential of prokaryotic IMP dehydrogenase inhibitors. *Curr Med Chem*. 2011;**18**:1909–18.

10 Chacko S, Boshoff HIM, Singh V, Ferraris DM, Gollapalli DR, Zhang M, et al. Expanding benzoxazole-based inosine 5'-monophosphate dehydrogenase (IMPDH) inhibitor structure-activity as potential antituberculosis agents. *J Med Chem*. 2018;**61**:4739–56.

11 Chen L, Wilson DJ, Xu Y, Aldrich CC, Felczak K, Sham YY, et al. Triazole-linked inhibitors of inosine monophosphate dehydrogenase from human and *Mycobacterium tuberculosis*. *J Med Chem*. 2010;**53**:4768–78.

12 Juvale K, Shaik A, Kirubakaran S. Inhibitors of inosine 5'-monophosphate dehydrogenase as emerging new generation antimicrobial agents. *MedChemComm*. 2019;**10**:1290–301.

13 Makowska-Grzyska M, Kim Y, Gorla SK, Wei Y, Mandapati K, Zhang M, et al. *Mycobacterium tuberculosis* IMPDH in complexes with substrates, products and antitubercular compounds. *PLoS One*. 2015;**10**:e0138976.

14 Sahu NU, Singh V, Ferraris DM, Rizzi M, Kharkar PS. Hit discovery of *Mycobacterium tuberculosis* inosine 5'-monophosphate dehydrogenase, GuaB2, inhibitors. *Bioorg Med Chem Lett*. 2018;**28**:1714–8.

15 Singh V, Donini S, Pacitto A, Sala C, Hartkoorn RC, Dhar N, et al. The inosine monophosphate dehydrogenase, GuaB2, is a vulnerable new bactericidal drug target for tuberculosis. *ACS Infect Dis*. 2017;**3**:5–17.

16 Usha V, Gurcha SS, Lovering AL, Lloyd AJ, Papaemmanouil A, Reynolds RC, et al. Identification of novel diphenyl urea inhibitors of Mt-GuaB2 active against *Mycobacterium tuberculosis*. *Microbiology*. 2011;**157**:290–9.

17 Sassetti CM, Boyd DH, Rubin EJ. Genes required for mycobacterial growth defined by high density mutagenesis. *Mol Microbiol*. 2003;**48**:77–84.

18 Sassetti CM, Boyd DH, Rubin EJ. Comprehensive identification of conditionally essential genes in mycobacteria. *Proc Natl Acad Sci USA*. 2001;**98**:12712–7.

19 Hedstrom L. The dynamic determinants of reaction specificity in the IMPDH/GMPR family of (beta/alpha)

(8) barrel enzymes. *Crit Rev Biochem Mol Biol*. 2012;**47**:250–63.

20 Hedstrom L. IMP dehydrogenase: structure, mechanism and inhibition. *Chem Rev*. 2009;**109**:2903–28.

21 Hedstrom L, Gan L. IMP dehydrogenase: structural schizophrenia and an unusual base. *Curr Opin Chem Biol*. 2006;**10**:520–5.

22 Ereno-Orbea J, Oyenarte I, Alfonso Martinez-Cruz L. CBS domains: ligand binding sites and conformational variability. *Arch Biochem Biophys*. 2013;**540**:70–81.

23 Nimmesgern E, Black J, Futer O, Fulghum JR, Chambers SP, Brummel CL, et al. Biochemical analysis of the modular enzyme inosine 5'-monophosphate dehydrogenase. *Protein Expr Purif*. 1999;**17**:282–9.

24 Gan L, Petsko GA, Hedstrom L. Crystal structure of a ternary complex of *Tritrichomonas foetus* inosine 5'-monophosphate dehydrogenase: NAD(+) orients the active site loop for catalysis. *Biochemistry*. 2002;**41**:13309–17.

25 Makowska-Grzyska M, Kim Y, Maltseva N, Osipiuk J, Gu M, Zhang M, et al. A novel cofactor-binding mode in bacterial IMP dehydrogenases explains inhibitor selectivity. *J Biol Chem*. 2015;**290**:5893–911.

26 Pimkin M, Markham GD. The CBS subdomain of inosine 5'-monophosphate dehydrogenase regulates purine nucleotide turnover. *Mol Microbiol*. 2008;**68**:342–59.

27 Pimkin M, Pimkina J, Markham GD. A regulatory role of the bateman domain of IMP dehydrogenase in adenylate nucleotide biosynthesis. *J Biol Chem*. 2009;**284**:7960–9.

28 Bessho T, Okada T, Kimura C, Shinohara T, Tomiyama A, Imamura A, et al. Novel characteristics of *Trypanosoma brucei* guanosine 5'-monophosphate reductase distinct from host animals. *PLoS Negl Trop Dis*. 2016;**10**:e0004339.

29 Sarwono AEY, Suganuma K, Mitsuhashi S, Okada T, Musinguzi SP, Shigetomi K, et al. Identification and characterization of guanosine 5'-monophosphate reductase of *Trypanosoma congolense* as a drug target. *Parasitol Int*. 2017;**66**:537–44.

30 Smith S, Boitz J, Chidambaram ES, Chatterjee A, Ait-Tihyaty M, Ullman B, et al. The cystathionine-beta-synthase domains on the guanosine 5'-monophosphate reductase and inosine 5'-monophosphate dehydrogenase enzymes from *Leishmania* regulate enzymatic activity in response to guanylate and adenylate nucleotide levels. *Mol Microbiol*. 2016;**100**:824–40.

31 Imamura A, Okada T, Mase H, Otani T, Kobayashi T, Tamura M, et al. Allosteric regulation accompanied by oligomeric state changes of *Trypanosoma brucei* GMP reductase through cystathionine-beta-synthase domain. *Nat Commun*. 2020;**11**:1837.

32 Magasanik B, Karibian D. Purine nucleotide cycles and their metabolic role. *J Biol Chem*. 1960;**235**:2672–81.

33 Patton GC, Stenmark P, Gollapalli DR, Sevastik R, Kursula P, Flodin S, et al. Cofactor mobility determines reaction outcome in the IMPDH and GMPR (beta-alpha)8 barrel enzymes. *Nat Chem Biol*. 2011;**7**:950–8.

34 Endo T, Uratani B, Freese E. Purine salvage pathways of *Bacillus subtilis* and effect of guanine on growth of GMP reductase mutants. *J Bacteriol*. 1983;**155**:169–79.

35 Benson CE, Gots JS. Regulation of GMP reductase in *Salmonella typhimurium*. *Biochim Biophys Acta*. 1975;**403**:47–57.

36 Kessler AI, Gots JS. Regulation of *guaC* expression in *Escherichia coli*. *J Bacteriol*. 1985;**164**:1288–93.

37 Griffin JE, Gawronski JD, Dejesus MA, Ioerger TR, Akerley BJ, Sassetti CM. High-resolution phenotypic profiling defines genes essential for mycobacterial growth and cholesterol catabolism. *PLoS Pathog*. 2011;**7**:e1002251.

38 DeJesus MA, Gerrick ER, Xu W, Park SW, Long JE, Boutte CC, et al. Comprehensive essentiality analysis of the *Mycobacterium tuberculosis* genome via saturating transposon mutagenesis. *MBio*. 2017;**8**:e02133-16.

39 Minato Y, Gohl DM, Thiede JM, Chacon JM, Harcombe WR, Maruyama F, et al. Genomewide assessment of *Mycobacterium tuberculosis* conditionally essential metabolic pathways. *mSystems*. 2019;**4**:e00070-19.

40 Rao M, Streur TL, Aldwell FE, Cook GM. Intracellular pH regulation by *Mycobacterium smegmatis* and *Mycobacterium bovis* BCG. *Microbiology (Reading)*. 2001;**147**:1017–24.

41 Vandal OH, Roberts JA, Odaira T, Schnappinger D, Nathan CF, Ehrt S. Acid-susceptible mutants of *Mycobacterium tuberculosis* share hypersusceptibility to cell wall and oxidative stress and to the host environment. *J Bacteriol*. 2009;**191**:625–31.

42 Zhang Y, Scorpio A, Nikaido H, Sun Z. Role of acid pH and deficient efflux of pyrazinoic acid in unique susceptibility of *Mycobacterium tuberculosis* to pyrazinamide. *J Bacteriol*. 1999;**181**:2044–9.

43 Knejzlik Z, Herkommerova K, Pichova I. Catabolism of 8-oxo-purines is mainly routed via the guanine to xanthine interconversion pathway in *Mycobacterium smegmatis*. *Tuberculosis*. 2019;**119**:101879.

44 Knejzlik Z, Herkommerova K, Hockova D, Pichova I. Hypoxanthine-guanine phosphoribosyltransferase is dispensable for *Mycobacterium smegmatis* viability. *J Bacteriol*. 2020;**202**:e00710-19.

45 Zbornikova E, Knejzlik Z, Hauryliuk V, Krasny L, Rejman D. Analysis of nucleotide pools in bacteria using HPLC-MS in HILIC mode. *Talanta*. 2019;**205**:120161.

46 Buey RM, Ledesma-Amaro R, Velazquez-Campoy A, Balsera M, Chagoyen M, de Pereda JM, et al. Guanine nucleotide binding to the bateman domain mediates the

allosteric inhibition of eukaryotic IMP dehydrogenases. *Nat Commun*. 2015;**6**:8923.

47 Johnson MC, Kollman JM. Cryo-EM structures demonstrate human IMPDH2 filament assembly tunes allosteric regulation. *Elife*. 2020;**9**:e53243.

48 Joyce AR, Reed JL, White A, Edwards R, Osterman A, Baba T, et al. Experimental and computational assessment of conditionally essential genes in *Escherichia coli*. *J Bacteriol*. 2006;**188**:8259–71.

49 Kobayashi K, Ehrlich SD, Albertini A, Amati G, Andersen KK, Arnaud M, et al. Essential *Bacillus subtilis* genes. *Proc Natl Acad Sci USA*. 2003;**100**:4678–83.

50 Salama NR, Shepherd B, Falkow S. Global transposon mutagenesis and essential gene analysis of *Helicobacter pylori*. *J Bacteriol*. 2004;**186**:7926–35.

51 Le Breton Y, Belew AT, Valdes KM, Islam E, Curry P, Tettelin H, et al. Essential genes in the core genome of the human pathogen *Streptococcus pyogenes*. *Sci Rep*. 2015;**5**:9838.

52 Deng Y, Wang Z, Ying K, Gu S, Ji C, Huang Y, et al. NADPH-dependent GMP reductase isoenzyme of human (GMPR2). Expression, purification, and kinetic properties. *Int J Biochem Cell Biol*. 2002;**34**:1035–50.

53 Martinelli LK, Ducati RG, Rosado LA, Breda A, Selbach BP, Santos DS, et al. Recombinant *Escherichia coli* GMP reductase: kinetic, catalytic and chemical mechanisms, and thermodynamics of enzyme-ligand binary complex formation. *Mol Biosyst*. 2011;**7**:1289–305.

54 Mitchell A, Sin IL, Finch LR. Enzymes of purine metabolism in *Mycoplasma mycoides* subsp. *mycoides*. *J Bacteriol*. 1978;**134**:706–12.

55 Spector T, Jones TE, Miller RL. Reaction mechanism and specificity of human GMP reductase. Substrates, inhibitors, activators, and inactivators. *J Biol Chem*. 1979;**254**:2308–15.

56 Heyde E, Nagabhushanam A, Vonarx M, Morrison JF. Studies on inosine monophosphate dehydrogenase – steady-state kinetics. *Biochim Biophys Acta*. 1976;**429**:645–60.

57 Kerr KM, Cahoon M, Bosco DA, Hedstrom L. Monovalent cation activation in *Escherichia coli* inosine 5'-monophosphate dehydrogenase. *Arch Biochem Biophys*. 2000;**375**:131–7.

58 Riera TV, Zheng L, Josephine HR, Min D, Yang W, Hedstrom L. Allosteric activation via kinetic control: potassium accelerates a conformational change in IMP dehydrogenase. *Biochemistry*. 2011;**50**:8508–18.

59 Rostirolla DC, Milech de Assunção T, Bizarro CV, Basso LA, Santos DS. Biochemical characterization of *Mycobacterium tuberculosis* IMP dehydrogenase: kinetic mechanism, metal activation and evidence of a cooperative system. *RSC Adv*. 2014;**4**:26271–87.

60 Xiang BS, Taylor JC, Markham GD. Monovalent cation activation and kinetic mechanism of inosine 5'-monophosphate dehydrogenase. *J Biol Chem*. 1996;**271**:1435–40.

61 Stephens RW, Whittaker VK. Calf thymus GMP reductase: control by XMP. *Biochem Biophys Res Commun*. 1973;**53**:975–81.

62 Goldbeck O, Eck AW, Seibold GM. Real time monitoring of NADPH concentrations in *Corynebacterium glutamicum* and *Escherichia coli* via the genetically encoded sensor mBFP. *Front Microbiol*. 2018;**9**:2564.

63 Vandal OH, Pierini LM, Schnappinger D, Nathan CF, Ehrt S. A membrane protein preserves intrabacterial pH in intraphagosomal *Mycobacterium tuberculosis*. *Nat Med*. 2008;**14**:849–54.

64 Darby CM, Ingolfsson HI, Jiang X, Shen C, Sun M, Zhao N, et al. Whole cell screen for inhibitors of pH homeostasis in *Mycobacterium tuberculosis*. *PLoS One*. 2013;**8**:e68942.

65 Peterson ND, Rosen BC, Dillon NA, Baughn AD. Uncoupling environmental pH and intrabacterial acidification from pyrazinamide susceptibility in *Mycobacterium tuberculosis*. *Antimicrob Agents Chemother*. 2015;**59**:7320–6.

66 Morimoto YV, Kami-Ike N, Miyata T, Kawamoto A, Kato T, Namba K, et al. High-resolution pH imaging of living bacterial cells to detect local pH differences. *MBio*. 2016;**7**:e01911-16.

67 Lu P, Haagsma AC, Pham H, Maaskant JJ, Mol S, Lill H, et al. Pyrazinoic acid decreases the proton motive force, respiratory ATP synthesis activity, and cellular ATP levels. *Antimicrob Agents Chemother*. 2011;**55**:5354–7.

68 Gengenbacher M, Rao SPS, Pethe K, Dick T. Nutrient-starved, non-replicating *Mycobacterium tuberculosis* requires respiration, ATP synthase and isocitrate lyase for maintenance of ATP homeostasis and viability. *Microbiology (Reading)*. 2010;**156**:81–7.

69 Rao SP, Alonso S, Rand L, Dick T, Pethe K. The protonmotive force is required for maintaining ATP homeostasis and viability of hypoxic, nonreplicating *Mycobacterium tuberculosis*. *Proc Natl Acad Sci USA*. 2008;**105**:11945–50.

70 Patil V, Jain V. Insights into the physiology and metabolism of a mycobacterial cell in an energy-compromised state. *J Bacteriol*. 2019;**201**:e00210-19.

71 Lamprecht DA, Finin PM, Rahman MA, Cumming BM, Russell SL, Jonnala SR, et al. Turning the respiratory flexibility of *Mycobacterium tuberculosis* against itself. *Nat Commun*. 2016;**7**:12393.

72 Dutta NK, Klinkenberg LG, Vazquez MJ, Segura-Carro D, Colmenarejo G, Ramon F, et al. Inhibiting the stringent response blocks *Mycobacterium tuberculosis* entry into quiescence and reduces persistence. *Sci Adv*. 2019;**5**:eaav2104.

73 Shenkerman Y, Elharar Y, Vishkautzan M, Gur E. Efficient and simple generation of unmarked gene deletions in *Mycobacterium smegmatis*. *Gene*. 2014;**533**:374–8.

74 Arnold FM, Hohl M, Remm S, Koliwer-Brandl H, Adenau S, Chusri S, et al. A uniform cloning platform for mycobacterial genetics and protein production. *Sci Rep*. 2018;**8**:9539.

75 Ehrt S, Guo XV, Hickey CM, Ryou M, Monteleone M, Riley LW, et al. Controlling gene expression in mycobacteria with anhydrotetracycline and Tet repressor. *Nucleic Acids Res*. 2005;**33**:e21.

76 Studier FW. Stable expression clones and auto-induction for protein production in *E. coli*. *Methods Mol Biol*. 2014;**1091**:17–32.

77 Wojdyr Marcin. *Fityk*: a general-purpose peak fitting program. *J Appl Crystallogr*. 2010;**43**:1126–8.

78 Mueller U, Forster R, Hellmig M, Huschmann FU, Kastner A, Malecki P, et al. The macromolecular crystallography beamlines at BESSY II of the Helmholtz-Zentrum Berlin: current status and perspectives. *Eur Phys J Plus*. 2015;**130**:141.

79 Kabsch W. XDS. *Acta Crystallogr D Biol Crystallogr*. 2010;**66**:125–32.

80 Krug M, Weiss MS, Heinemann U, Mueller U. XDSAPP: a graphical user interface for the convenient processing of diffraction data using XDS. *J Appl Crystallogr*. 2012;**45**:568–72.

81 Zhang RG, Evans G, Rotella FJ, Westbrook EM, Beno D, Huberman E, et al. Characteristics and crystal structure of bacterial inosine-5'-monophosphate dehydrogenase. *Biochemistry*. 1999;**38**:4691–700.

82 Emsley P, Lohkamp B, Scott WG, Cowtan K. Features and development of Coot. *Acta Crystallogr D Biol Crystallogr*. 2010;**66**:486–501.

83 Afonine PV, Grosse-Kunstleve RW, Echols N, Headd JJ, Moriarty NW, Mustyakimov M, et al. Towards automated crystallographic structure refinement with phenix.refine. *Acta Crystallogr D Biol Crystallogr*. 2012;**68**:352–67.

84 Liebschner D, Afonine PV, Baker ML, Bunkoczi G, Chen VB, Croll TI, et al. Macromolecular structure determination using X-rays, neutrons and electrons: recent developments in Phenix. *Acta Crystallogr D Struct Biol*. 2019;**75**:861–77.

85 Williams CJ, Headd JJ, Moriarty NW, Prisant MG, Videau LL, Deis LN, et al. MolProbity: more and better reference data for improved all-atom structure validation. *Protein Sci*. 2018;**27**:293–315.

86 Altschul SF, Gish W, Miller W, Myers EW, Lipman DJ. Basic local alignment search tool. *J Mol Biol*. 1990;**215**:403–10.

87 Yang M, Derbyshire MK, Yamashita RA, Marchler-Bauer A. NCBI's conserved domain database and tools for protein domain analysis. *Curr Protoc Bioinformatics*. 2020;**69**:e90.

88 Dereeper A, Guignon V, Blanc G, Audic S, Buffet S, Chevenet F, et al. Phylogeny.fr: robust phylogenetic analysis for the non-specialist. *Nucleic Acids Res*. 2008;**36**:W465–9.

89 Edgar RC. MUSCLE: multiple sequence alignment with high accuracy and high throughput. *Nucleic Acids Res*. 2004;**32**:1792–7.

90 Castresana J. Selection of conserved blocks from multiple alignments for their use in phylogenetic analysis. *Mol Biol Evol*. 2000;**17**:540–52.

91 Guindon S, Gascuel O. A simple, fast, and accurate algorithm to estimate large phylogenies by maximum likelihood. *Syst Biol*. 2003;**52**:696–704.

92 Letunic I, Bork P. Interactive Tree Of Life (iTOL) v5: an online tool for phylogenetic tree display and annotation. *Nucleic Acids Res*. 2021;**49**:W293–6.

93 Jones P, Binns D, Chang HY, Fraser M, Li W, McAnulla C, et al. InterProScan 5: genome-scale protein function classification. *Bioinformatics*. 2014;**30**:1236–40.

94 Anisimova M, Gascuel O. Approximate likelihood-ratio test for branches: a fast, accurate, and powerful alternative. *Syst Biol*. 2006;**55**:539–52.